AD-A155 612 AN INVESTIGATION INTO THE COMPARISONS OF THE UNDERWATER SHOCK EFFECTS ON A.. (U) NAVAL POSTGRADUATE SCHOOL MONTEREY CA J R LANGAN MAR 85 1/1

UNCLASSIFIED F/G 18/3 NL

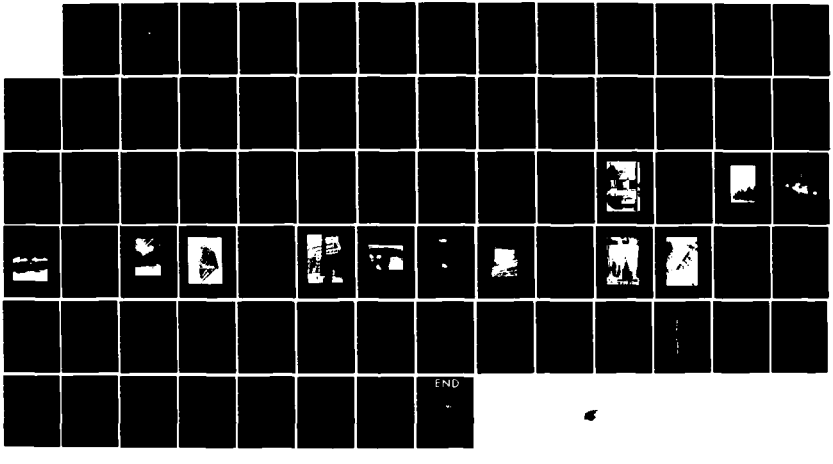

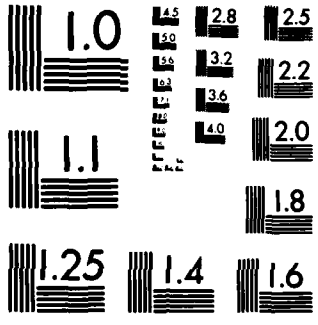

MICROCOPY RESOLUTION TEST CHART
NATIONAL BUREAU OF STANDARDS-1963-A

(2)

NAVAL POSTGRADUATE SCHOOL
Monterey, California

THESIS

AN INVESTIGATION INTO THE COMPARISONS OF THE UNDERWATER SHOCK EFFECTS ON A STIFFENED FLAT PLATE TO THE PREDICTIVE NATURE OF A COMPUTER MODEL

by

John R. Langan

March 1985

Thesis Advisor: Y.S. Shin

Approved for public release; distribution unlimited

UNCLASSIFIED

SECURITY CLASSIFICATION OF THIS PAGE (When Data Entered)

REPORT DOCUMENTATION PAGE		READ INSTRUCTIONS BEFORE COMPLETING FORM
1. REPORT NUMBER	2. GOVT ACCESSION NO.	3. RECIPIENT'S CATALOG NUMBER
4. TITLE (and Subtitle) An Investigation into the Comparisons of the Underwater Shock Effects on a Stiffened Flat Plate to the Predictive Nature of a Computer Model		5. TYPE OF REPORT & PERIOD COVERED Master's Thesis March 1985 6. PERFORMING ORG. REPORT NUMBER
7. AUTHOR(s) John R. Langan		8. CONTRACT OR GRANT NUMBER(s)
9. PERFORMING ORGANIZATION NAME AND ADDRESS Naval Postgraduate School Monterey, California 93943		10. PROGRAM ELEMENT, PROJECT, TASK AREA & WORK UNIT NUMBERS
11. CONTROLLING OFFICE NAME AND ADDRESS Naval Postgraduate School Monterey, California 93943		12. REPORT DATE March 1985 13. NUMBER OF PAGES 74
14. MONITORING AGENCY NAME & ADDRESS(if different from Controlling Office)		15. SECURITY CLASS. (of this report) Unclassified 15a. DECLASSIFICATION/ DOWNGRADING SCHEDULE

16. DISTRIBUTION STATEMENT (of this Report)

Approved for public release; distribution unlimited.

17. DISTRIBUTION STATEMENT (of the abstract entered in Block 20, if different from Report)

18. SUPPLEMENTARY NOTES

19. KEY WORDS (Continue on reverse side if necessary and identify by block number)

Stiffener Tripping,
Flat Plate Underwater Shock Response.

20. ABSTRACT (Continue on reverse side if necessary and identify by block number)

An experiment was performed to study the effects of an underwater explosion on a submerged test panel. This is a part of an on-going research project sponsored by the Defense Nuclear Agency (DNA) to help predict the dynamic responses of naval structural members due to underwater shocks. An important element of this thesis was to validate a finite element/finite central difference computer code developed to forecast shell

DD FORM 1 JAN 73 1473 EDITION OF 1 NOV 65 IS OBSOLETE

S N 0102-LF-014-6601

UNCLASSIFIED

SECURITY CLASSIFICATION OF THIS PAGE (When Data Entered)

#20 - ABSTRACT - (CONTINUED)

responses. Emphasis was placed upon attaining stiffener tripping and collecting invaluable dynamic flat plate tripping data.

Approved for public release; distribution is unlimited.

An Investigation into the Comparisons of the Underwater Shock Effects on a Stiffened Flat Plate to the Predictive Nature of a Computer Model

by

John R. Langan
Lieutenant Commander, United States Navy
B.S., United States Naval Academy, 1975

Submitted in partial fulfillment of the requirements for the degree of

MASTER OF SCIENCE IN MECHANICAL ENGINEERING

from the

NAVAL POSTGRADUATE SCHOOL

March 1985

Author: John R. Langan
John R. Langan

Approved by:
Y. S. Shin, Thesis Advisor

Paul J. Marto, Chairman
Department of Mechanical Engineering

John N. Dyer,
Dean of Science and Engineering

ABSTRACT

An experiment was performed to study the effects of an underwater explosion on a submerged test panel. This is a part of an on-going research project sponsored by the Defense Nuclear Agency (DNA) to help predict the dynamic responses of naval structural members due to underwater shocks. An important element of this thesis was to validate a finite element/finite central difference computer code developed to forecast shell responses. Emphasis was placed upon attaining stiffener tripping and collecting invaluable dynamic flat plate tripping data.

TABLE OF CONTENTS

LIST OF TABLES

LIST OF FIGURES

ACKNOWLEDGEMENT

I would like to express my deep appreciation and thanks to the many people who made this thesis a reality. First to Professor Shin for the motivation and guidance provided throughout this project. Secondly, to Dr. Raymond Daddazio for his willingness to assist and the many hours he spent in running the EPSA computer code. Next, to the superb support staff at NPS; Tom McCord for his coordinating efforts, the "electrical guru," Tom Christian, for his special electronics package and infamous San Francisco driving skills, and Charles Crowe for his countless hours of test structure fabrication. And finally, to my best buddy--my wife, Joanne, whose love, patience and determination has inspired me to tackle this institution and has lightened my load.

I. INTRODUCTION

A. OBJECTIVES

Current building specifications for U.S. Navy ships and submarines require shock to be met on shipboard equipment and that underwater shock testing be performed on at least one ship in each class [Ref. 1]. Underwater explosion (UNDEX) research is conducted at NPS because of the importance of shock testing to the Navy. The objectives of this thesis are four-fold. First, to investigate the large deflection elasto-plastic transient response characteristics of submerged stiffened flat plates, subjected to underwater shock. Secondly, to perform underwater explosion testing using a stiffened flat plate and to validate the predicted results with those of the experiment. Thirdly, to investigate stiffener tripping and its effect to the gross shell responses. And finally, to acquire the knowledge and technical expertise necessary to conduct these types of experiments.

What is stiffener tripping and why is it significant to naval construction? Stiffener tripping is defined as the lateral-torsional instability of a stiffener as it becomes suddenly unstable and fails under load [Ref. 2]. Tripping is identified by a twisting of the stiffener about its line of attachment to a structure. The purpose of stiffeners is to add strength to ship hulls. Removal of the stiffener

weakens the structure. A report published in 1979 by John Adamchak stresses the importance of stiffener tripping effects on shipboard hulls and grillages by stating that previous underwater tests

> clearly demonstrate the significance of lateral-torsional instability (tripping) as a primary ductile failure mode for a ship's structure. [Ref. 2]

Once a stiffened structure has experienced tripping, its ability to continue to resist deformation under loading is drastically reduced.

B. BACKGROUND

This is the third NPS thesis in the field of UNDEX and their dynamic effects on submerged plates. This research is part of a major project coordinated and sponsored by the Defense Nuclear Agency. During the early part of 1984, Lt. Tom Rentz conducted the first NPS thesis research on UNDEX responses of flat plates. A plate positioned on top of an air-backed test platform was chosen to best simulate the conditions present in ship hulls.

Fabrication and exact specifications of the test platform are covered in detail in [Ref. 3], with Figure 1.1 showing a sketch of this structure. Flat plates are manufactured out of 6061-T6 aluminum because it is accessible, easy to machine and this material exhibits strain rate independent properties. The first plate tested is shown in Figure 1.1 and consisted of two parallel rectangular bar

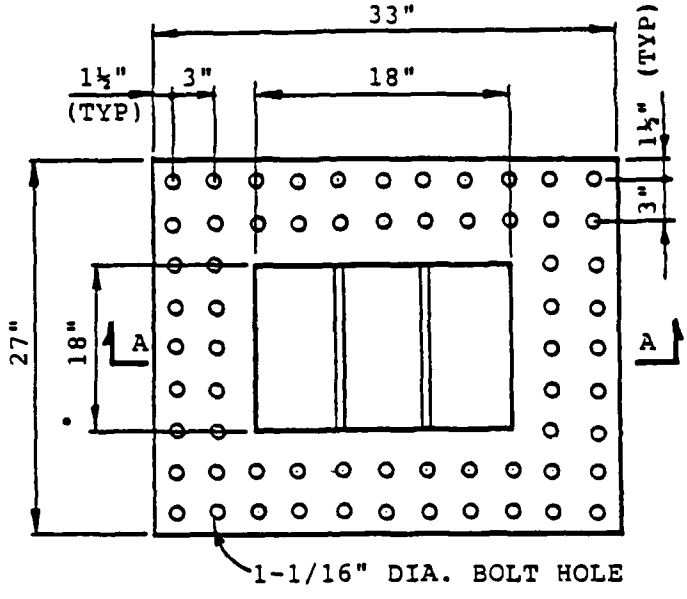

PLAN VIEW

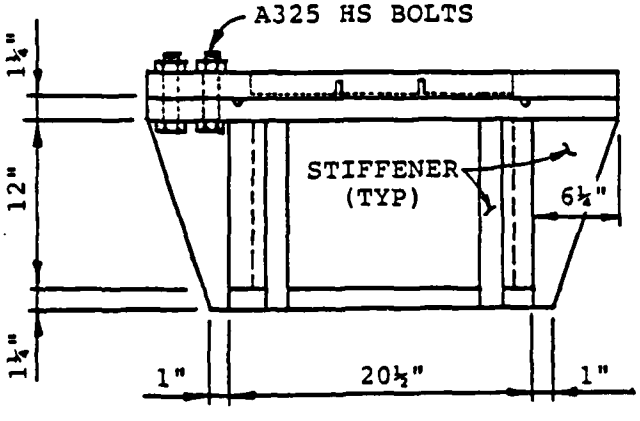

ELEVATION VIEW

NOTE: MATERIAL OF BACKING STRUCTURE IS A36 STEEL AND PLATE THICKNESS IS 1½".

Figure 1.1 Test Structure Drawing

stiffeners with a thickness of 0.1875 inches and height of 1.0 inches running transversely on the plate.

In February 1984, an explosive shot was performed on the first stiffened plate. Last-minute changes made it necessary for sixteen half-pound rectangular blocks of TNT to be substituted for a single eight-pound charge. Test results revealed large deformations and tears at stiffener ends which prevented stiffener tripping.

Lt. Nelson King was the next to pursue the area of UNDEX at NPS. During the summer months of 1984, he performed two explosions, using different plate designs for each. His first plate was similar to Figure 1.1 except that the stiffeners were reconfigured to a tee, see Figure 1.2. It was believed by exposing more surface area to the shock

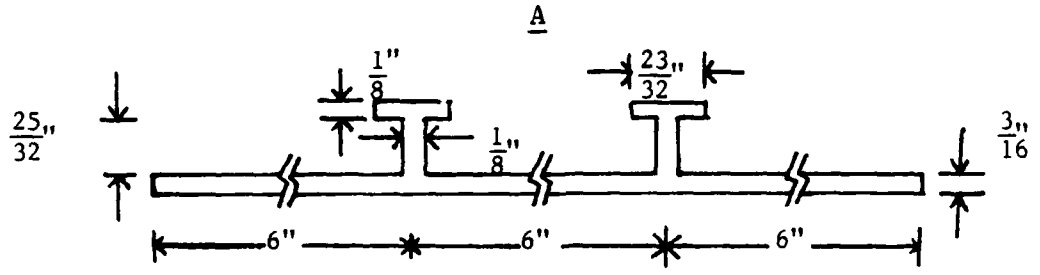

Figure 1.2 King's Tee-shaped Stiffener

wave, a larger compression zone would be developed, encouraging tripping. A single nine and a half-pound test charge was exploded. Test results were similar to the first explosion. A move towards a simpler test panel was taken.

The test panel was redesigned to a single bar stiffener with increased thickness to 0.25 inches and height to 1.25 inches running longitudinally. Figure 1.3 shows the geometry of this new panel. A half-pound charge of TNT was exploded over the test plate. Recorded sensor results were invalid for this experiment but micrometer measurements taken later indicated that perhaps a slight amount of stiffener bowing was taking place and further testing with this test geometry was warranted [Ref. 4].

The test panel investigated for this thesis is identical to the single longitudinal stiffener model. A charge weight of eight pounds TNT, a depth of four feet and a plate stand-off distance of nine feet was selected. The experiment was conducted at West Coast Shock Facility (WCSF) at Hunter's Point Shipyard, California.

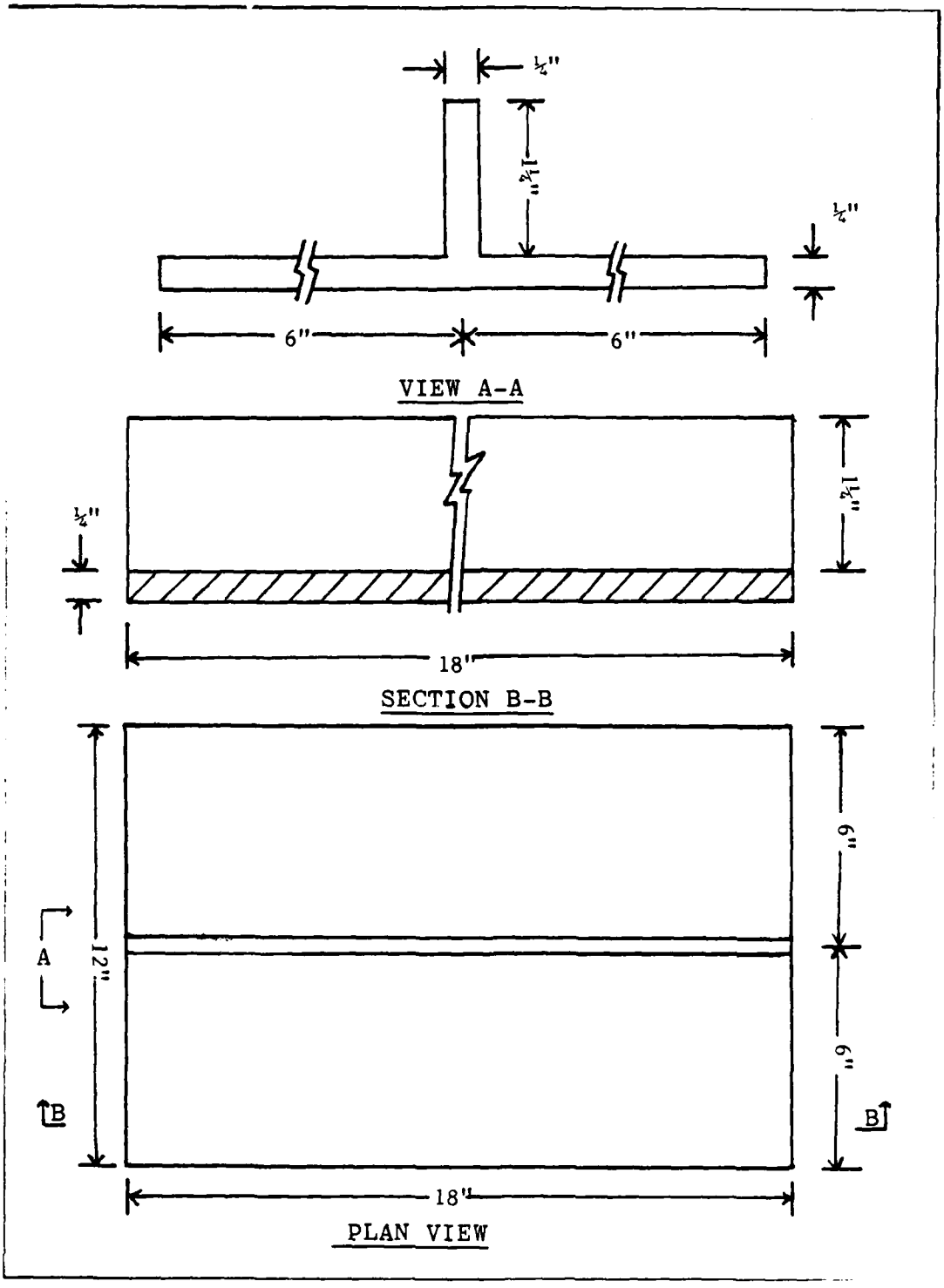

Figure 1.3 King's Plate and Current Model

II. UNDERWATER EXPLOSION THEORY

Before continuing with the experimental aspect of this research, an overview of UNDEX theory is provided. Explosions are a very complex field of study. The destructive effect of an explosion is dependent upon the composition and geometry of the explosive element, the media or surrounding environment, the stand-off distance to the target and the physical nature of the target. Simply stated, an explosion is a chemical reaction which releases energy; both thermal and mechanical [Ref. 5].

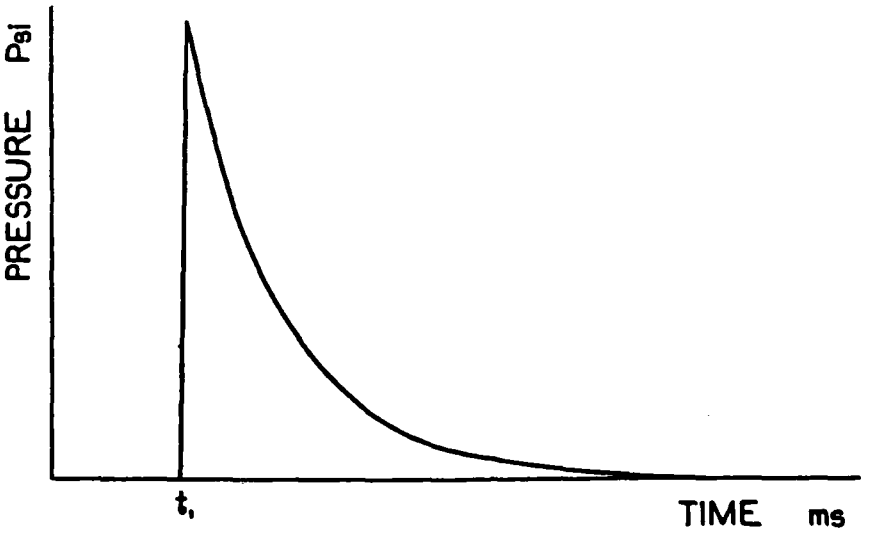

Figure 2.1 Shock Wave Pressure Profile

A. THE SHOCK WAVE

An immediate result of underwater detonation is a high gas pressure build-up. The gases interact with the surrounding water causing compression and a radial outward flow. This forms the shock wave which comprises about half of the explosion's energy. It is the effects of the shock wave on the flat plate that is the primary area of interest for this thesis research. The exact character of the shock wave near the charge is not well known, thus, focus will be on the characteristics of the shock wave at some distance away. Experience has shown that the shock wave travels at the speed of sound in water (approximately 5000 feet per second) [Ref. 6]. Formulas have been developed for distances between 10 and 100 times the charge's radius to describe such features as: peak pressure, pressure as a function of time, and time decay constant. Ideally, the shock wave, which delivers a pressure incident, has a profile similar to Figure 2.1. There is a sharp peak pressure spike, followed by an exponential decay, with about one third the original pressure occurring after only a single time decay constant.

A few equations useful in the description of the shock wave pressure profile are listed below. Pressure is described by equation 2.1.

$$P(t) = P_{max} e^{-\frac{(t-t_1)}{\theta}} \quad ; \quad \text{given} \quad t > t_1 \quad \text{psi} \qquad (2.1)$$

θ is the explosive decay constant and P_{max} is peak pressure given by equations 2.2 and 2.3.

$$\theta = K_2 W^{1/3} \left(\frac{W^{1/3}}{R}\right)^{A_2} \quad \text{msec} \qquad (2.2)$$

$$P_{max} = K_1 \left(\frac{W^{1/3}}{R}\right)^{A_1} \quad \text{psi} \qquad (2.3)$$

The time of shock wave arrival at the target, T, is calculated from equation 2.4.

$$T = \frac{R}{C} \quad \text{sec} \qquad (2.4)$$

where:

W is explosive weight in pounds

R is stand-off in feet from charge to target

$t-t_1$ is elapsed time after shock's arrival

A_1, A_2, K_1 and K_2 are constants which vary depending on the type of explosive (see Table I)

C is the speed of sound in water

The experimental values expected for an eight-pound charge of TNT with a nine foot target stand-off are peak pressure of 3814 psi, decay constant of 0.153 msec and shock arrival time of 1.8 msec.

TABLE I

Explosive Constants

Explosive	TNT	HBX-1	Pentolite
K_1	22,505	22,347.6	24,589
A_1	1.18	1.144	1.194
K_2	.058	.056	.052
A_2	-.185	-.247	-.257
K_3	12.67	14.14	12.88
K_4	4.268	4.761	4.339

In order to obtain clean data the secondary effects of UNDEX had to be eliminated or reduced. UNDEX secondary effects to a target include gas bubble, bulk cavitation, and surface and bottom reflection effects. A description of each of these phenomena is provided.

B. THE GAS BUBBLE

The gas bubble is an UNDEX phenomenon which is closely related to the shock wave. At detonation, while the shock wave flows radially outward, the highly compressed gases form a bubble which expands in size with an accompanying decrease of bubble gas pressure. The internal gas pressure gradually decays as the bubble expands until hydrostatic pressure finally takes over forcing the bubble to contract. Bubble contraction is slow at first but progresses rapidly until a minimum bubble radius is attained. The bubble eventually collapses producing a pressure pulse which stimulates

radial flow outward forming a new bubble that initiates the cycle all over again. Pressure pulses continue to be produced until all of the bubble energy is emitted. These pulses make up part of the reloading nature of an underwater explosion. Although the bubble pressure pulses are significantly weaker in magnitude than the incident shock wave (on the order of 10-15 percent of the first bubble pulse), they still represent important dynamic loads to a target [Ref. 7].

An interesting aspect of gas bubble theory is the migration of the bubble to the surface. The migration is upward due to the influence of gravity, with the most rapid changes noticed when the bubble's volume is at a minimum. Figure 2.2 depicts the relationship between bubble expansion, pressure pulse emissions and bubble migration. This figure is adapted from [Ref. 7]. Experiments have shown that the energy associated with the gas bubble is about 41 percent of the total energy available during an explosion [Ref. 1]. The following empirical formulas are presented to give some appreciation for the gas bubble and its behavior. The maximum bubble radius and the period of the first pressure pulse are given by equations 2.5 and 2.6.

$$A_{max} = K_3 \frac{W^{1/3}}{(D+33)^{1/3}} \quad \text{ft.} \qquad (2.5)$$

$$T = K_4 \frac{W^{1/3}}{(D+33)^{5/6}} \quad \text{sec} \qquad (2.6)$$

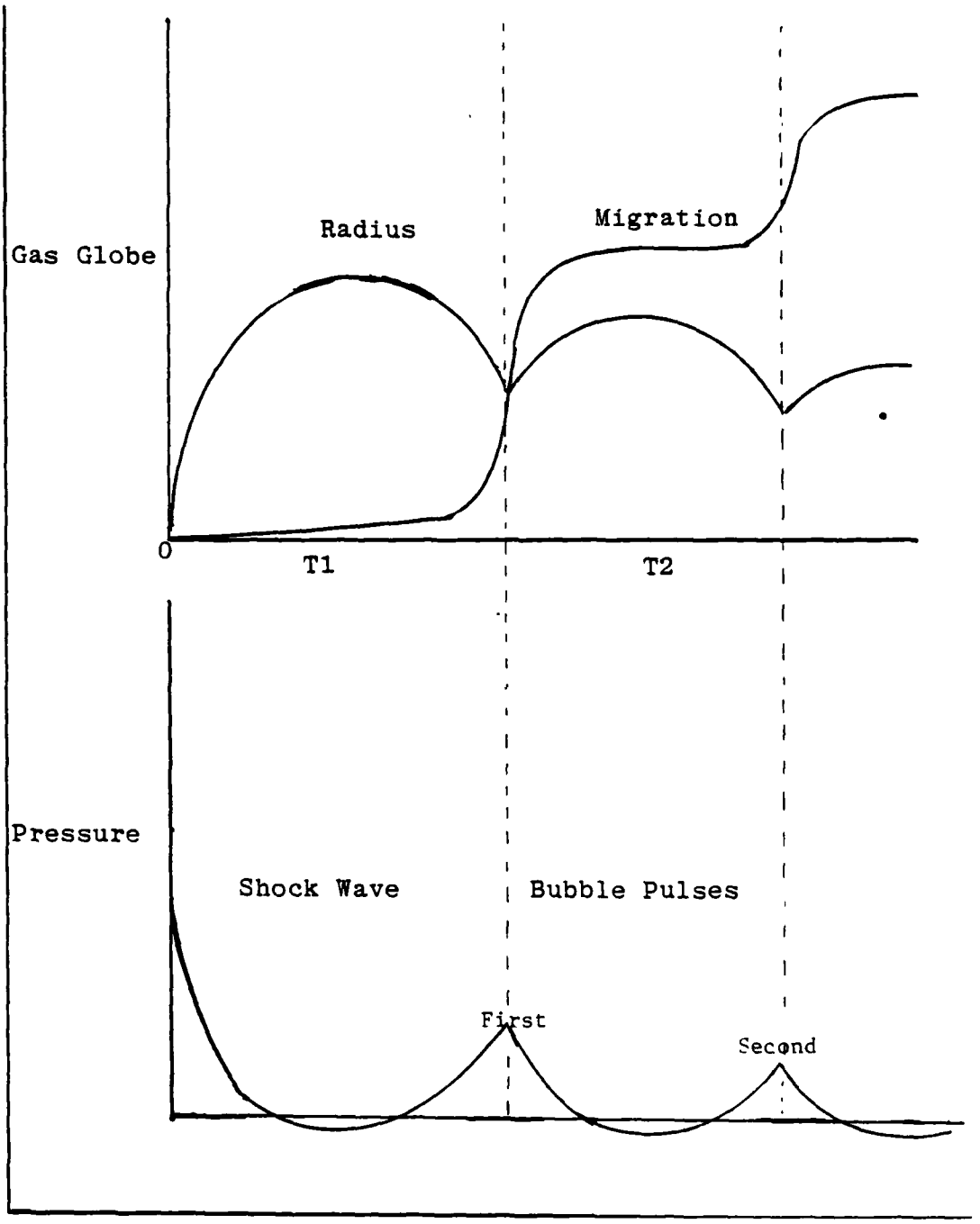

Figure 2.2 Bubble Historical Representation

where:

A_{max} is maximum bubble radius

K_3 and K_4 are constants from Table I

D is the submerged charge depth in feet

Both of these equations employ the fact that the pressure at the surface of the water is one atmosphere or 33 feet of sea water.

C. BULK CAVITATION ZONE

Bulk cavitation is an area where air bubbles or pockets have formed which are a result of the reflection of the compressive shock wave off the water's surface. As the shock wave reflects from a free surface it changes in sign to a tension wave. The water mass eventually pulls apart beneath the free surface to prevent any further tension and voids are created [Ref. 6]. The parameters which affect the area of the bulk cavitation zone are charge type, weight and depth.

D. FREE SURFACE AND BOTTOM REFLECTIONS

Free surface and bottom reflections are termed 'late-time' effects. The shock wave moves radially outward from the charge, very much like the resultant water motion from a pebble thrown into a still pond. The incident shock wave proceeds directly to the target, while the bottom and free surface serve as boundaries or obstructions. Surface cut-off

occurs at the target when the reflected free surface negative pressure wave strikes. To help visualize what is happening with surface reflection, an image source is used. Figure 2.3 shows the assumed image source, charge and point of interest/ target. Figure 2.4 depicts the type of pressure profile experienced by the target. Using the geometry of Figure 2.3, surface cut-off time and pressure can be computed by equations 2.7 and 2.8. Both of these figures are taken from [Ref. 1].

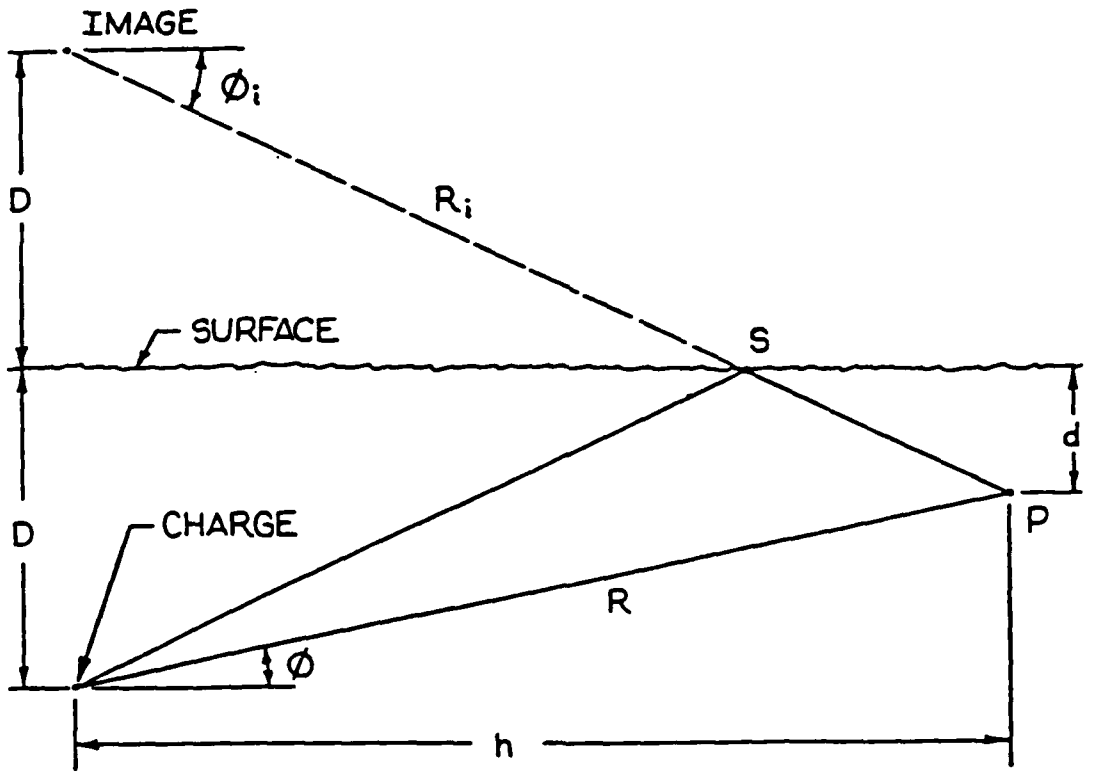

Figure 2.3 Image Source

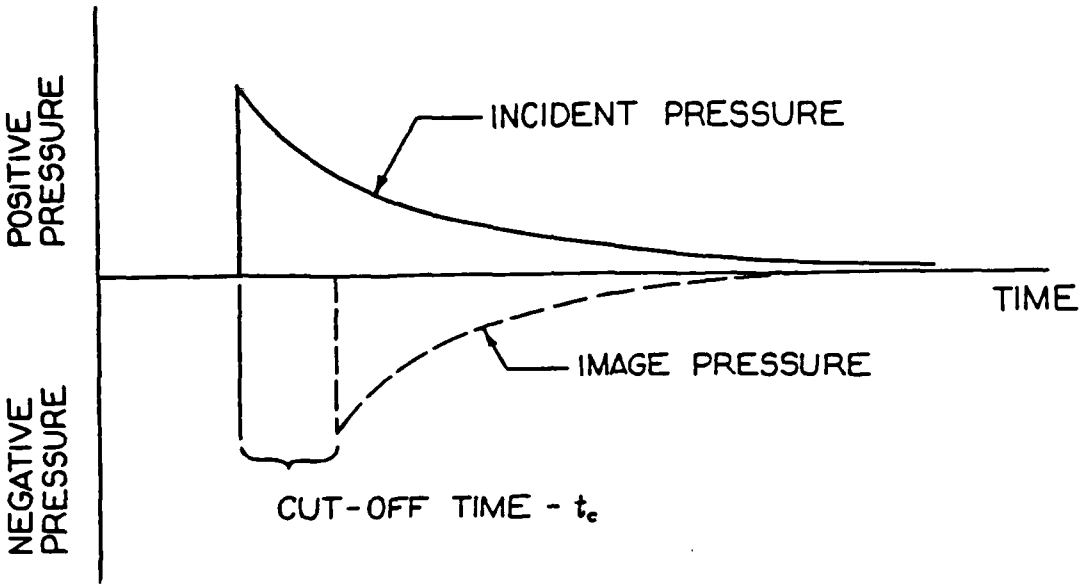

Figure 2.4 Incident and Surface Reflected Pressure Waves

$$t_c = \frac{R_i - R}{C} \quad \text{sec} \qquad (2.7)$$

$$P_c = -K_1 \left(\frac{W^{1/3}}{R_i}\right)^{A_1} \quad \text{psi} \qquad (2.8)$$

where:

R_i and R are expressed in feet

C is speed of sound--500 fps

The influences of the sea bed or bottom are not as well understood as those of the surface. However, the bottom is considered to be a perfectly rigid boundary reflecting waves

back with the same sign and magnitude. This is really an approximation as pointed out in [Ref. 6]. Figure 2.5 obtained from [Ref. 9] is used to graphically incorporate the effects of the shock wave, surface and bottom reflection pressure waves striking the point of interest.

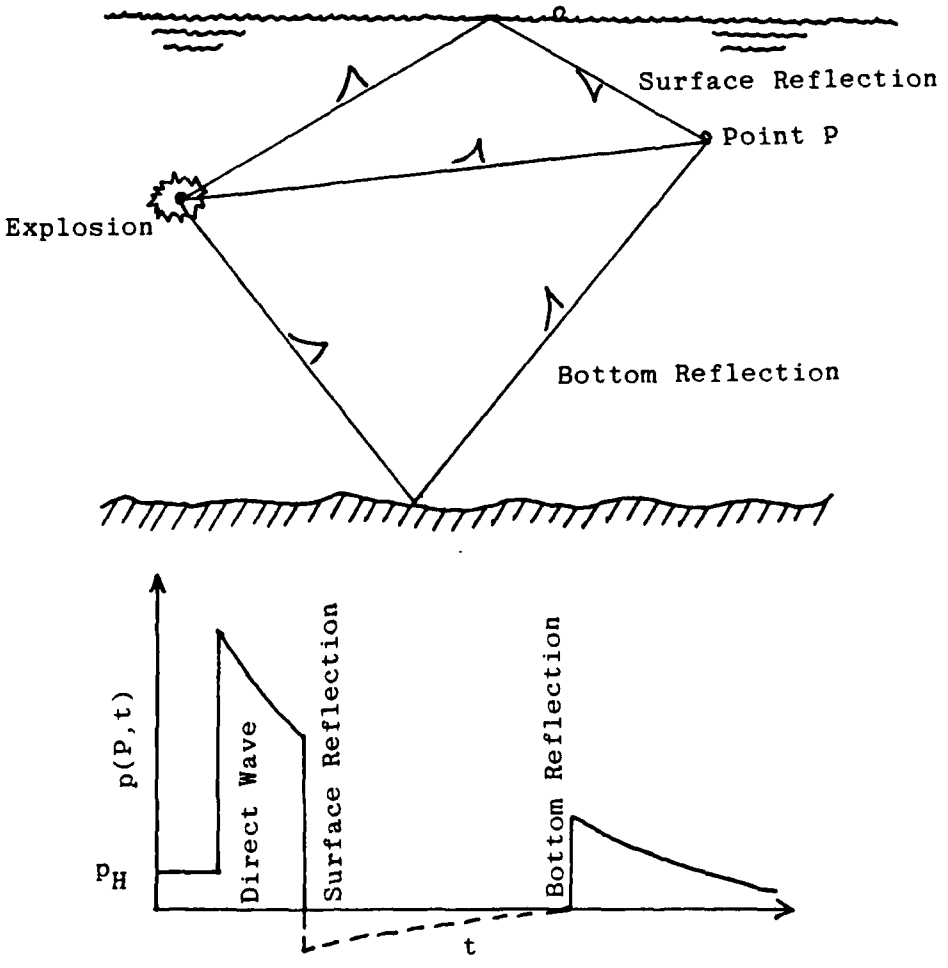

Figure 2.5 Shock Wave Interactions

E. EXPERIMENTAL CONDITIONS AND PRE-SHOT CALCULATIONS

As mentioned earlier one of the objectives of this thesis was to obtain clean data, looking primarily at the effects of the incident shock wave. By careful attention to test platform positioning in the water, most of the secondary effects could be eliminated. A charge depth of four feet was selected which allowed for adequate venting of the gas bubble to the atmosphere prior to hitting the test plate. Additionally, experience has shown that a satisfactory venting depth is one which is between 50 and 80 percent of maximum gas bubble radius [Ref. 1]. Using equation 2.5, a maximum bubble radius of 7.6 feet was computed. This represents a depth to radius ratio of 52.6%.

To eliminate bulk cavitation, the cavitation region had to be first determined. The equations necessary to calculate this region are extensive and tedious, thus a computer program was used to graph the cavitated region, see Figure 2.6. To avoid bulk cavitation and in keeping with past NPS UNDEX experiments, a nine feet stand-off distance was used.

Bottom and surface reflections are late time effects. By positioning the test structure directly beneath the charge, there is a time window of approximately 2.5 msec where reflections can be ignored. The experiments' sensors were sampled during this time frame. The depth of the water at the test site is approximately thirty feet.

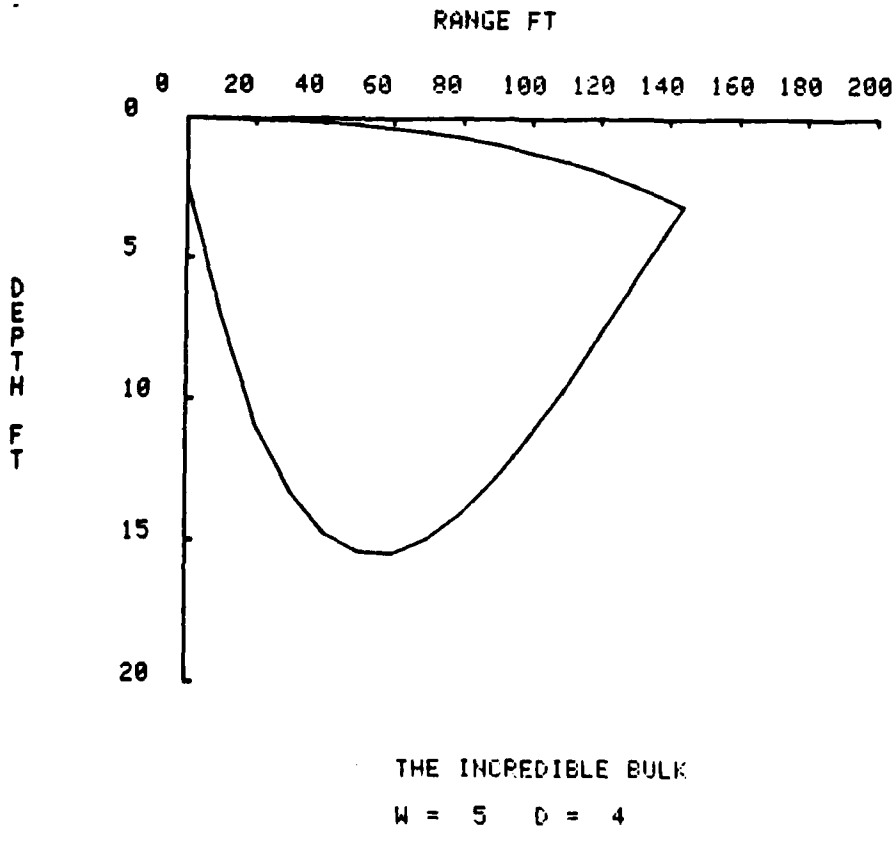

Figure 2.6 Bulk Cavitation Zone

III. THE COMPUTER CODE

The computer code selected for use in this thesis is EPSA, Elasto-Plastic Shell Analysis, developed by Weidlinger Associates. This is the second attempt at NPS to model a flat plate based on the EPSA code. Lt. Rentz was the first to utilize EPSA, see [Ref. 3].

EPSA is a finite element, finite central difference computer code. For calculation purposes EPSA assumes a symmetric loading pattern and time zero commences when the spherical shock wave first encounters the test plate. DNA/NAVSEA funded its development for the purpose of analyzing dynamic loading effects on submerged stiffened shells. The theory incorporated in EPSA is explained in the EPSA User's Manual [Ref. 8].

The purpose of this chapter is to describe how EPSA was used in the pre-shot calculations for this experiment. In Chapter V, EPSA will be reviewed emphasizing its post-experiment capabilities. EPSA is operated on a Vax-11/780 computer system located in Spanagel Hall.

Symmetry conditions were incorporated to model the aluminum test plate for EPSA, see Figure 3.1. Requiring only half of the plate to be discretized saved on computer time and storage space. EPSA computes quantities from nodal points and elements. Plate displacements and pressures are nodal point values, whereas stresses and strains are elemental.

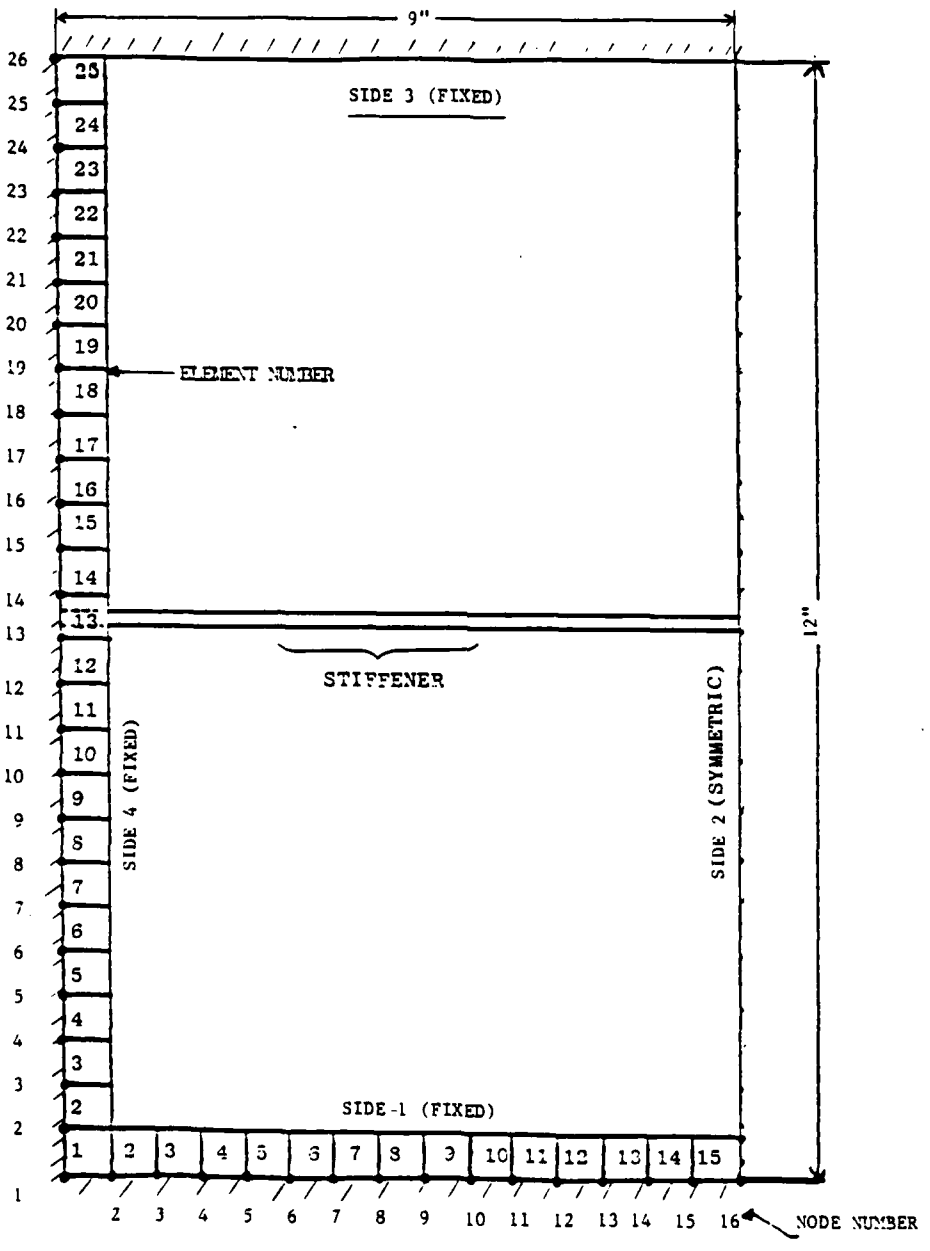

Figure 3.1 Half Plate EPSA Discretization Model

Selecting a discretization of fifteen columns by twenty five rows yielded rectangular block sizes of 0.6 by 0.48 inches. The total number of elements and nodes are 375 and 416, respectively. Sides one, three, and four have fixed boundary conditions and side two represents a symmetry edge.

A computer data deck is necessary to run the EPSA code. A sample data deck created for this thesis is reproduced in Figure 3.2. The User's Manual describes in detail the information included in this input deck. It is through the input deck that the plate physical characteristics and the underwater experimental conditions are passed to the computer code.

To facilitate in the viewing of EPSA output files, Francois Daube, a thesis student, wrote an interface program with PATRAN-G. PATRAN provides a color graphics capability for the display of von Mises' stresses and plate displacements at requested time increments. Daube's work is presented in [Ref. 10] and the EPSA-PATRAN interface is covered in [Ref. 3].

A color chronological history of von Mises' stresses and displacements for an eight-pound TNT charge was created. By looking at PATRAN and EPSA, pre-shot outputs strain gage locations were selected. See Figure 3.3. Emphasis was placed upon positioning the gages in an X,Y orientation and maintaining symmetry in order to compare experimental loading patterns to EPSA predictions.

```
JL PLATE
2500 1 0 0 0 10 0 0 1 1
.0000017
15 25 4 1 1 0 3 1 1 15 1 1 0
0 0
10000000. .5 .000255 40000. .1875 0. .00001
'STIF' 1 1 0
-1 1 2
416 0
1 0 0 0. 0.
16 1 0 4. 0.
-16 16 25 0 .18
0/
375 1 1 15 25
1 1 15 1 1 1 1 0
2 1 25 1 0 0 1 0
3 1 15 1 1 1 1 0
4 1 25 1 1 1 1 0
1 1 1 1 0. 1. 0.
0./
16 1 1 16 1 2 16 1 3/
15 1 1/
15 1 7/
3 4 3 8 4 3 16 4 3 3 7 3 6 7 3
16 7 3 3 13 3 9 13 3 16 13 3 3 12 3
8 12 3 16 12 3 3 20 3 8 21 3 16 20 3/
.48 .250 1.25
13 1/
0/
0.0      0.0010345    60000.0
1     110.156540    0.0554245      0.1
8.0    22510.0    1.18    0.158   -0.185  0.0012/
0/
```

Figure 3.2   A Sample EPSA Computer Deck

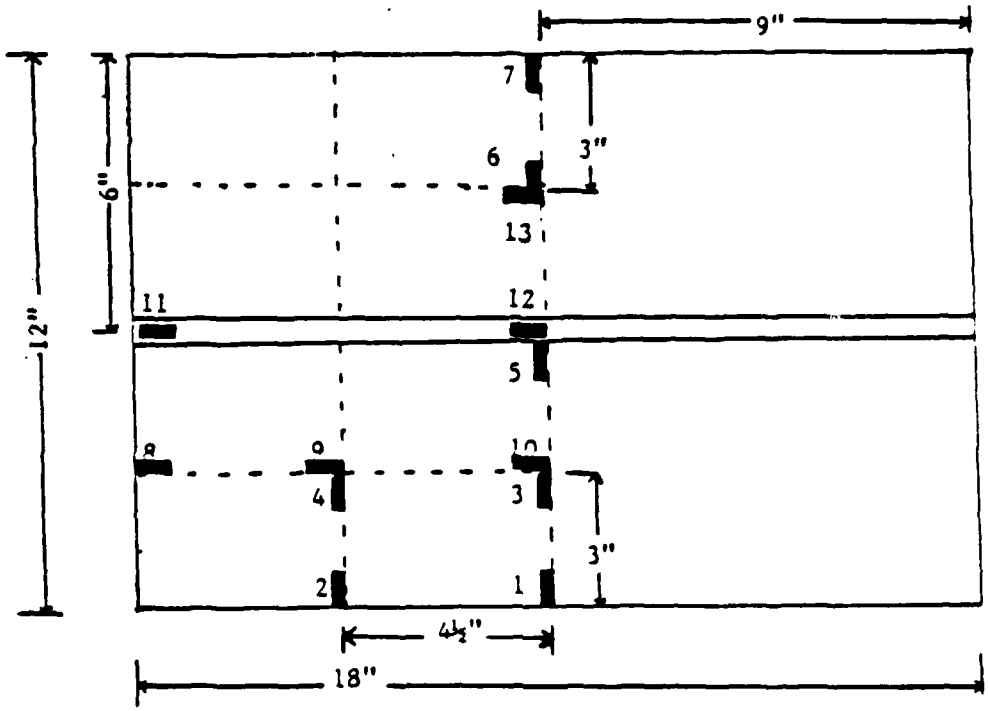

Figure 3.3 Strain Gage Locations

IV. UNDERWATER SHOCK TESTING

A. INSTRUMENTATION

The UNDEX experiment was conducted at the West Coast Shock Facility (WCSF). This is a Navy sponsored activity accessible to NPS, located about 120 miles to the north, in the South Bay of San Francisco.

Thirteen strain gages, two accelerometers and two pressure transducers were installed on the test structure. The location of the strain gages has already been shown on Figure 3.3. The accelerometers were mounted alongside each other at the bottom of the test structure. One of the pressure transducers was placed on a nine foot arc from the charge approximately five feet away from the test platform to record incident pressure data. This was secured in place by light manila guidelines and anchored vertically by a weight. The other was situated on top of the plate coming out of one of the corners at a 45° angle towards the plate's center. This transducer served as the basis for the plate's total pressure measurements. The sensor specifications are listed in Table II.

Two Honeywell M101 Wideband II (direct record) tape units operating at 120 inches-per-second recorded all data channels. On-site verification of data was accomplished with a Honeywell 1508b Visicorder. Post-processing of the data was through

TABLE II

Instrumentation Specifications

EQUIPMENT	TYPE	MAX RANGE
Strain gages	CEA-350 ohms	50,000 microstrains
Pressure gages	.25" Tourmaline	10 kpsi, 97% Response Ratio
Accelerometers	PCB Piezoelectric	2500 and 100,000 G's
Amplifiers	Ektron 563FJ	---

an HP-5451C Fourier Analyzer located at NPS. A schematic of the instrumentation is shown in Figure 4.1. To assist in data reviewing, an ingenious triggering mechanism was devised by electronic technician Tom Christian. This triggering device consisted of a small DC circuit wrapped around the charge. At time of detonation the wire breaks registering a zero voltage reading on the recorder.

Instrumentation wires ran down from the connection box on the test structure, along the bay's floor to the WCSF's instrumentation shack. Figure 4.2 is a photo of the Honeywell recorders and their associated amplifiers in the electronic's shack. It should be noted that a redesigned connection box was constructed and implemented for this shot. On the previous UNDEX experiments a brass electrical box was installed, which did not afford adequate protection to the connections. To remedy this weakness, a new box was fabricated out of 1.25 inch, A36 structural steel plate.

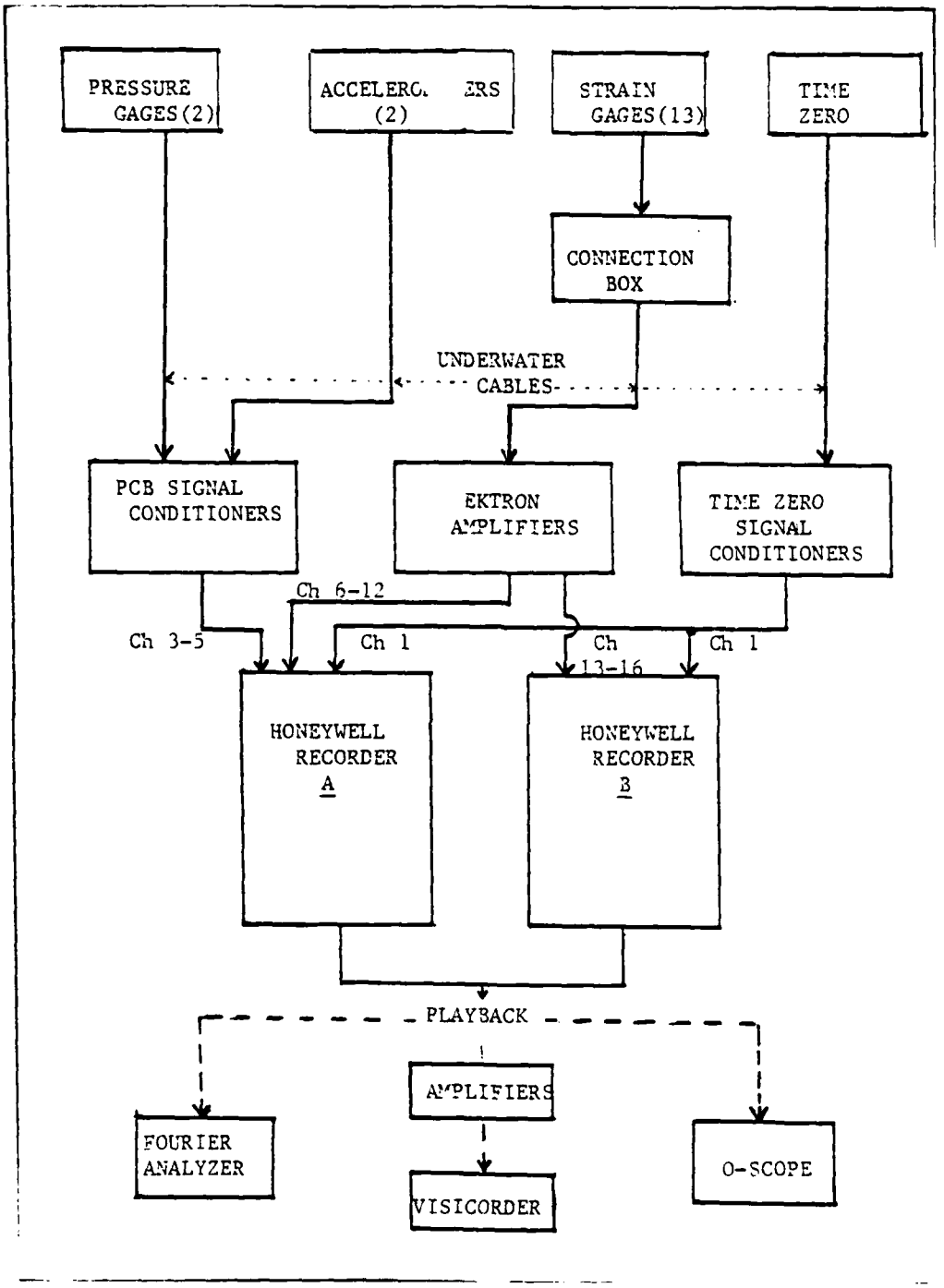

Figure 4.1 Instrumentation Schematic

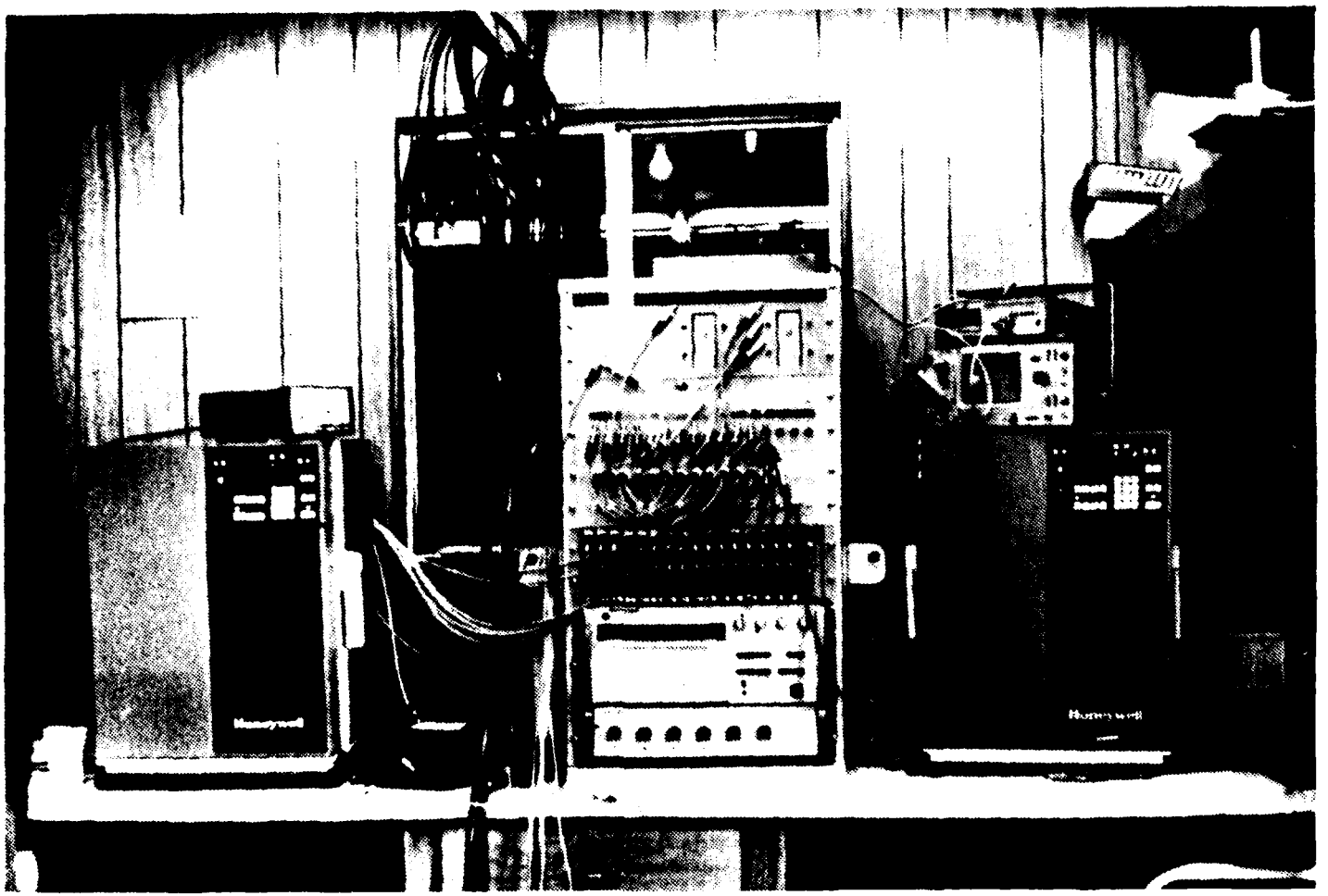

Figure 4.2 Honeywell Recorder and Amplifiers

B. SHOT DAY

Thursday, 6 December 1984, was set as the shot date. A drawing of the test rig is provided by Figure 4.3. The

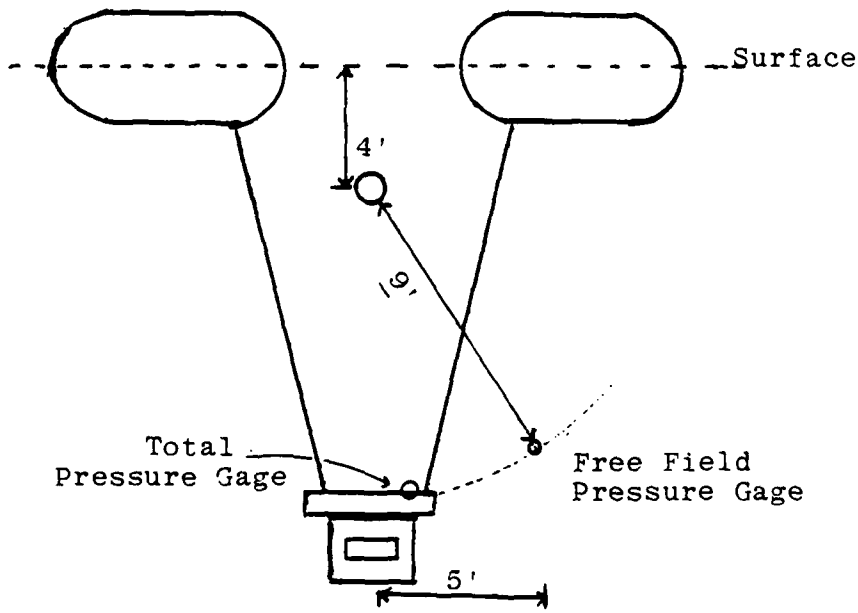

Figure 4.3 Test Rig Model

weather was ideal for an UNDEX experiment--clear and sunny skies, calm seas and no wind. After re-examining the equipment and performing calibration checks on the sensors, the riggers took over preparing the test structure for the bay. Figures 4.4, 4.5, and 4.6 show the shot sequence. Immediately after the explosion, everyone sensed something had gone wrong

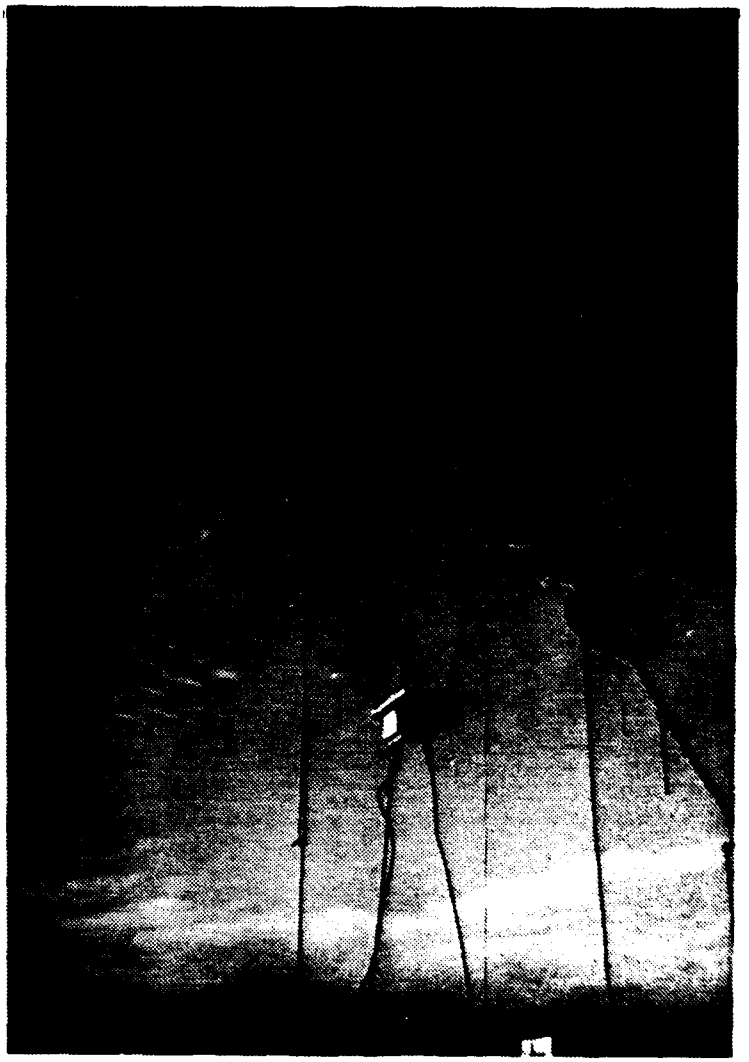

Figure 4.4 Crane Hoisting Test Panel

Figure 4.5 Test Panel Submerged/Boom Removal

Figure 4.6 First Explosion

with the shot as the water plume was smaller than expected, and the explosive sound was muffled. Tom Christian, stationed in the instrumentation shack, yelled out moments later that he had picked up some very weak signals on all channels, but was unsure of their meaning. Figure 4.7 reveals the test structure as it is being hauled out of the water following the explosion. No significant external damage was apparent and it was noticed that the free field pressure transducer was intact and still properly oriented. It was not until the test structure was repositioned on dock, that a large amount of unexploded TNT was discovered on top of the plate, see Figure 4.8. The appearance of the TNT on the plate was conclusive that the full eight-pounds of explosive did not go off. The unexploded residue was collected and weighed approximately one and a half pounds. During post-analysis, by examining the pressure graphs from the Fourier Analyzer, it was determined that approximately 0.16 pounds of TNT actually exploded. This was obtained by inputting the recorded value of 820 psi into equation 2.3 and solving for charge weight.

The plate surface was carefully inspected with no visible damages noted. Deflection measurements were not taken as a micrometer was not available. The electrical connection box remained water-tight and all but one of the sensors were still operational. After a short deliberation and determining the availability of another eight-pound charge, it was decided to fire another shot later that same day. WCSF

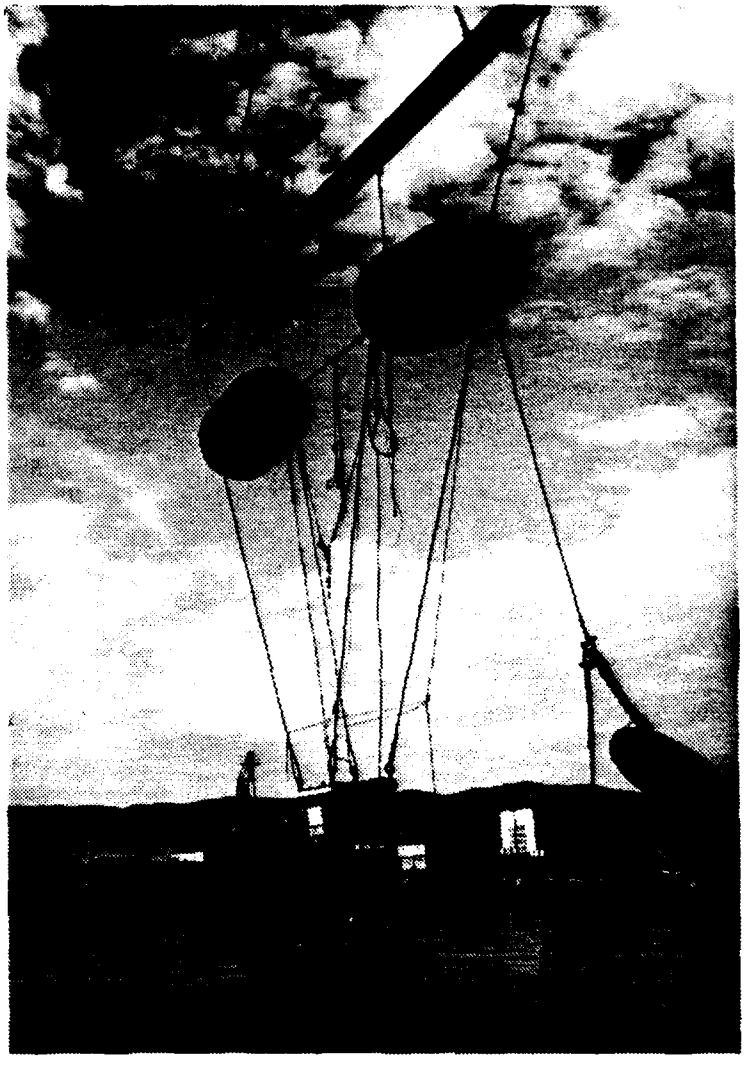

Figure 4.7 Test Structure After First Explosion

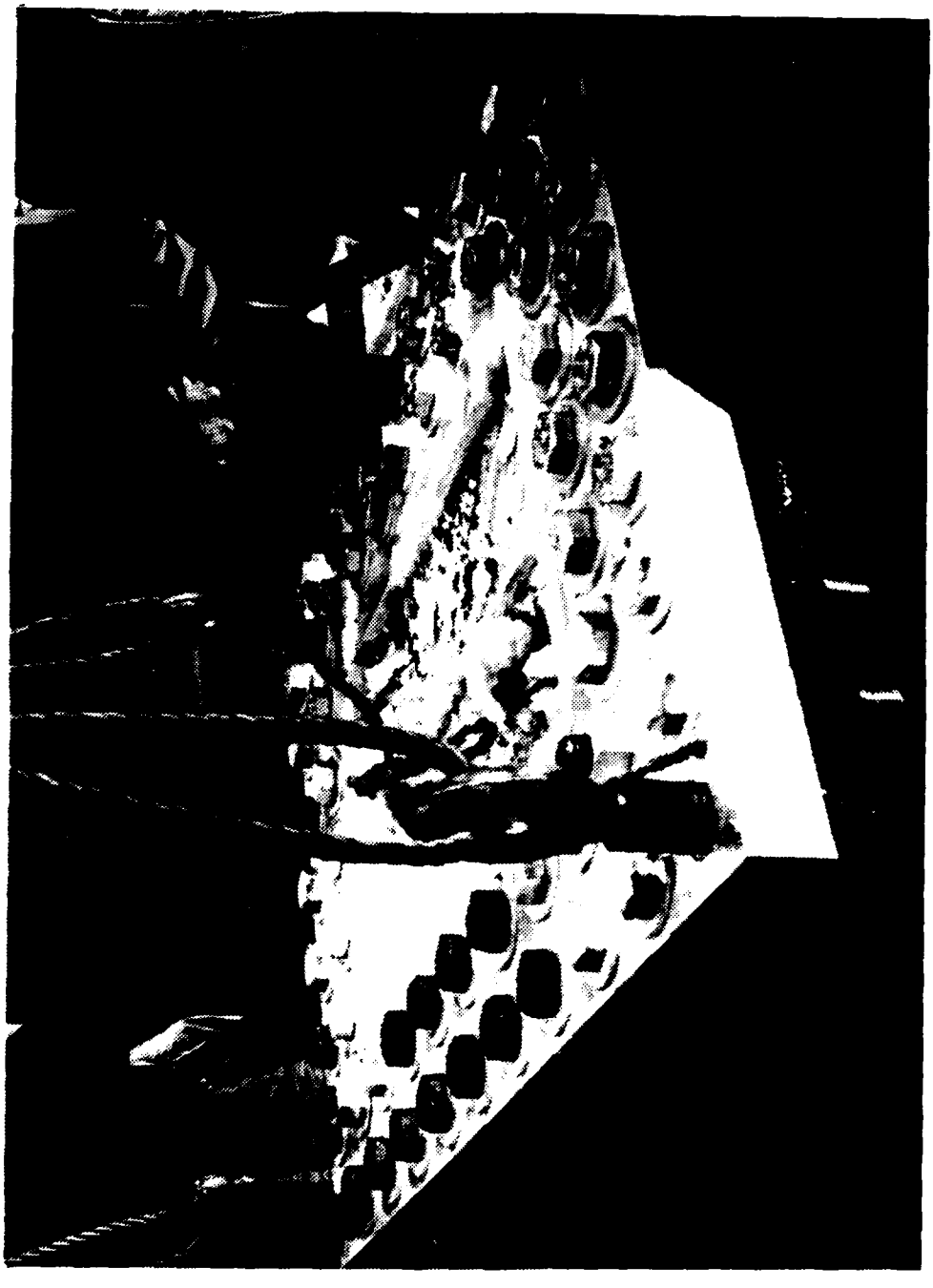

Figure 4.8 Unexploded TNT from the First Shot

personnel had stated that this was the first incomplete explosion of this type they had experienced. Incidentally, it should be pointed out that firing a small primer charge before a larger explosion is not an uncommon practice. Experience has shown that a primer tends to aid in gage calibration and loosens up residual plate stresses.

Approximately three hours later, another explosion occurred. This time two blasting caps were used to ensure full detonation of the TNT. It was apparent from the noise and water plume that the second shot was significantly larger than the early one. It was later determined from pressure data graphs that the peak pressure pulse experienced by the plate for this second shot was 4217 psi, which is equivalent to a 9.84 pound TNT charge. Figure 4.9 shows the water plume produced by the second shot. One of the pneumatic bladders ruptured from the force of the explosion, as shown in Figure 4.10. Another post shot view, Figure 4.11, shows the damage experienced by the test rig. Notice how two of the test platform support cables have been torn free.

A view of the underside of the test structure and cable runs going into the electrical connection box is shown in Figure 4.12. In the past the electrical cables have been pulled loose from the box, exposing the connections to the environment. Following this second explosion, Tom Christian joyfully announced that data had been collected.

Figure 4.9 Water Plume from the Second Shot

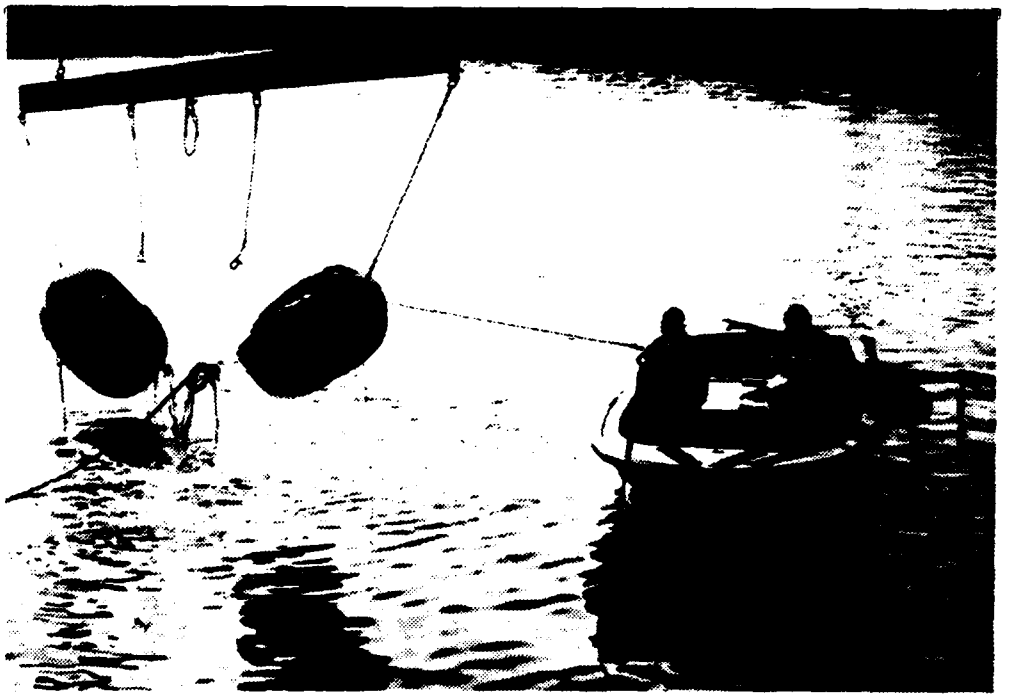

Figure 4.10 Ruptured Pneumatic Bladder

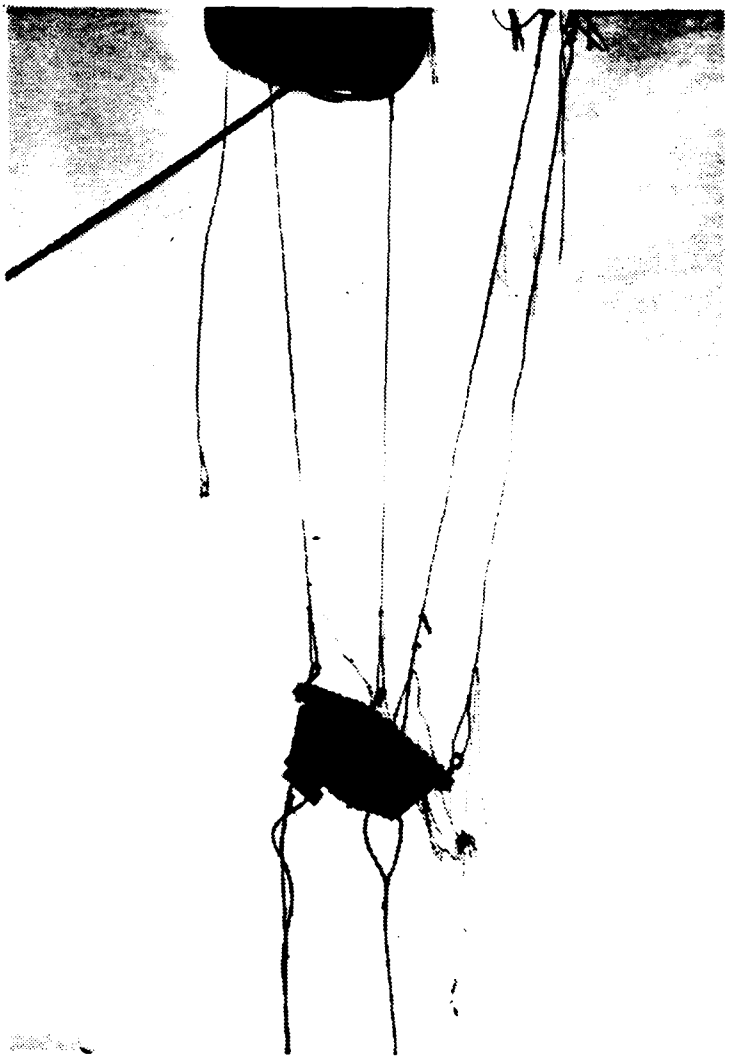

Figure 4.11 Post Shot View of Test Rig

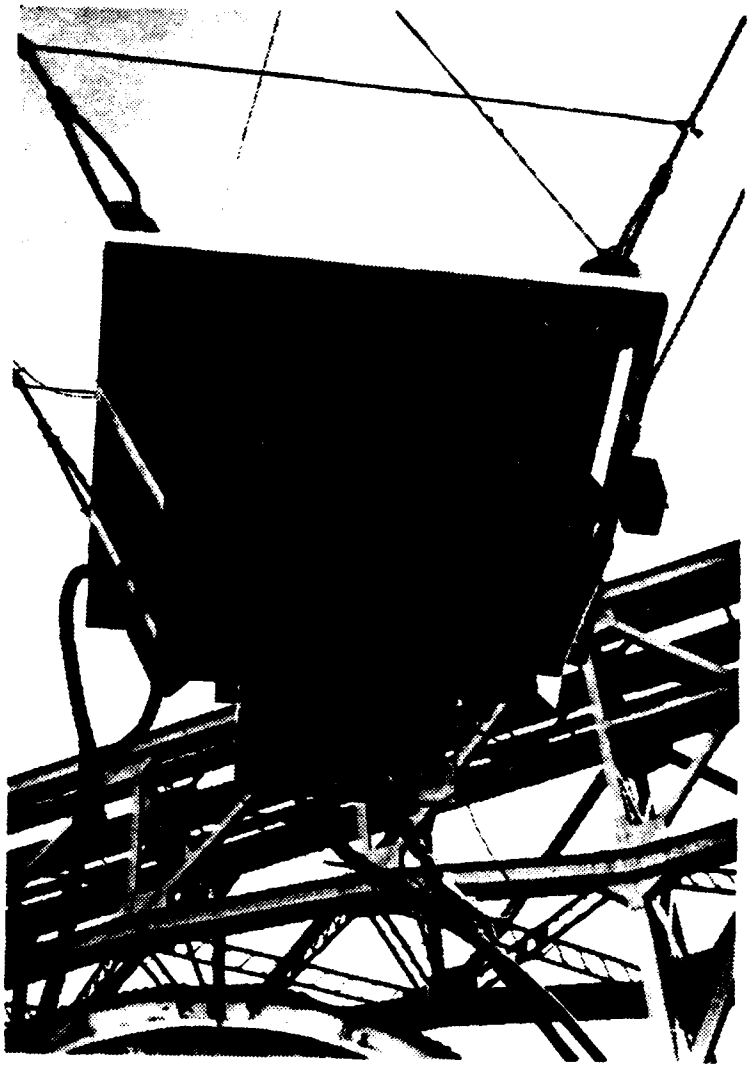

Figure 4.12 Clamped Cable Run into Connection Box

V. RESULTS AND RECOMMENDATIONS

A. PHYSICAL RESULTS

As mentioned in Chapter IV, the first shot did not produce any noticeable physical results. However, the second shot did achieve large deformations as evidenced by Figures 5.1 and 5.2. Both stiffener's ends sheared and there are tears along three of the sides. The exact tear lengths are recorded on Figure 5.3. Not visible in any of the photos is the fact that several strain gages became detached from the plate surface during the testing. Additionally, a few of the strain gage lead wires were severed. This severing was probably due to a guide wire shackle that parted from the ruptured flotation device following the shot.

Dial indicator deflection readings were taken while the aluminum plate was still clamped to the test structure, and are presented in Figure 5.3. An EPSA run was made using a 9.84 pound TNT charge to determine predicted deflections. EPSA predicted and actual displacements are compared on Figure 5.3. There are large discrepancies noticed in these comparisons, especially near locations where plate tears exist. EPSA does not take into account possible secondary effects which may have loaded the plate, most notably the loading generated by water particles striking the plate due to the downward rigid body action of the test structure.

Figure 5.1 Shearing at Both Stiffener Ends

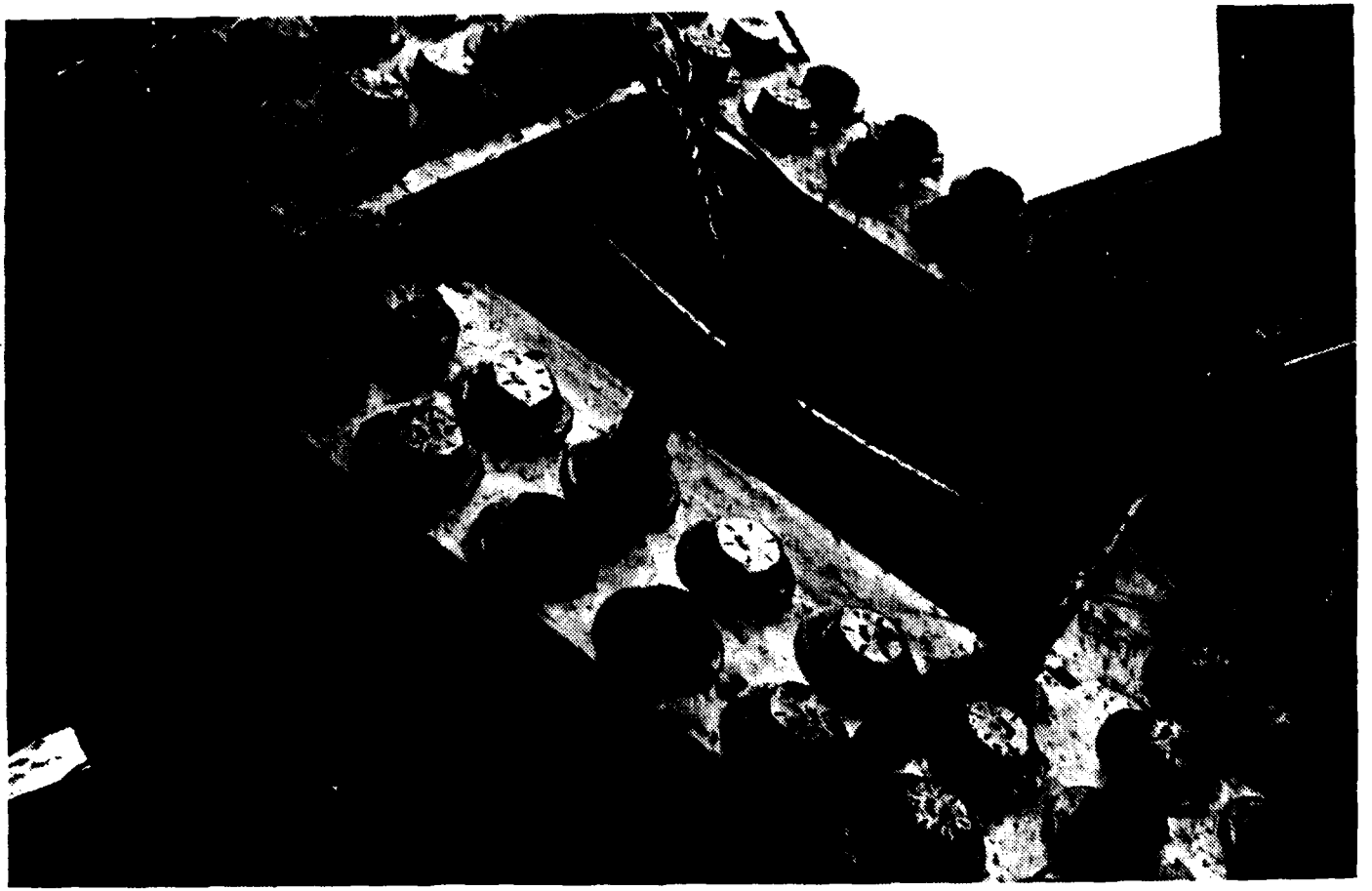

Figure 5.2 Large Plate Tear at the Side

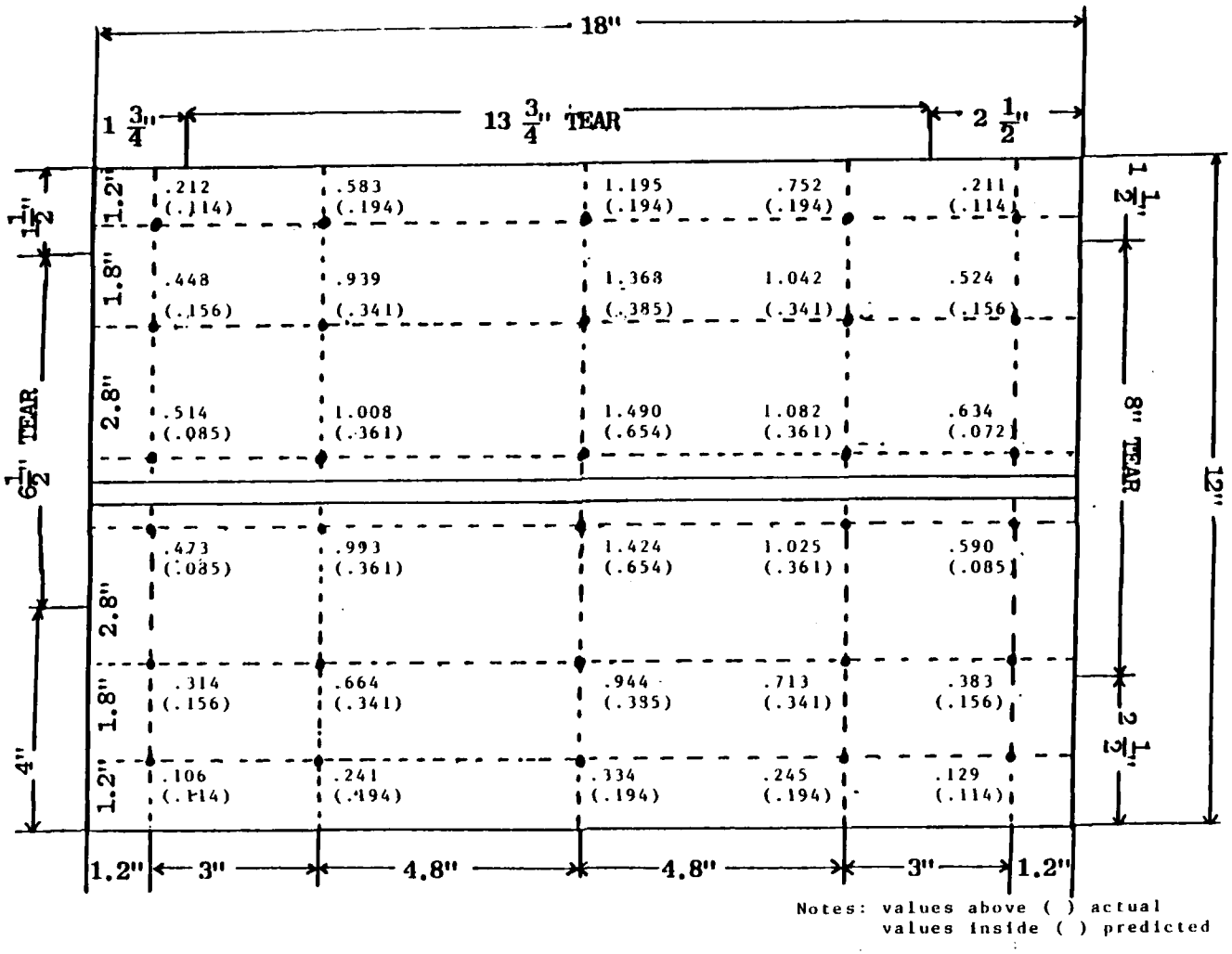

Figure 5.3 Displacement-EPSA 9.84 lbs TNT Predicted vs Actual

EPSA assumes a perfectly symmetric loading pattern, without any stress concentrators and does not incorporate fracture mechanics.

B. DATA INTERPRETATION

The majority of data interpretation was conducted at NPS using the HP-5451C Fourier Analyzer. Sensor data recorded on FM tape was transferred from the Honeywell recorder to a 5451C disk. All channel data was recorded at 120 inches-per second (ips) and played back to the disk at 1.875 ips. A real time conversion factor of 64 is necessary to change from 120 to 1.875 ips. Time zero for data reduction purposes is the exact moment of detonation. The triggering channel was instrumental and served as a reference in transferring data from the recorder to the disk. All seventeen channels are permanently stored both on tape and disk at NPS. Each data channel consists of fifteen storage records, with each record tracking 20.47 msec at 1.875 ips time or 0.319 msec real time.

Table III gives a summary of data, storage locations and conversion scale factors used for shots one and two. Sample digitized output data graphs are provided in Appendix A. Time was not available to write a computer program to change the scales on the axes to reflect proper units or actual times. However, reference values are indicated on each graph.

As mentioned earlier, the digitized incident pressure data from shot one yielded a peak pressure of 820 psi,

TABLE III

Recorded Sensor Data

SHOT #1

SENSOR	STORED	CONVERSION SCALE	PEAK VALUES	ARRIVAL TIME
A2 X"	91-105	100 k	(.046 v) 4.6 kG's	3.02 msec
A3 X"	106-120	100 k	(.054 v) 5.46 kG's	3.01 msec
A4 P(t)	121-135	10 k	(.058 v) 585 psi	2.11 msec
A5 P(f)	136-150	20 k	(.041 v) 820 psi	1.95 msec
A6 SG1	NO DATA COLLECTED			
A7 SG2	1-15	40 k	(3.31 v) 132 kμstrains	2.31 msec
A8 SG3	16-30	10 k	(.113 v) 1.13 kμstrains	2.16 msec
A9 SG4	31-45	10 k	(.074 v) .743 kμstrains	2.16 msec
A10 SG5	46-60	10 k	(.046 v) .469 kμstrains	2.20 msec
A11 SG6	61-75	10 k	(.052 v) .527 kμstrains	2.18 msec
A12 SG7	76-90	10 k	(.060 v) .606 kμstrains	2.28 msec
SG8-SG13	NO DATA COLLECTED			

SHOT #2

A2 X"	151-165	100 k	(2.64 v) 264 kG's	3.11 msec
A3 X"	166-180	100 k	(1.88 v) 188 kG's	3.03 msec
A4 P(t)	181-195	10 k	(.492 v) 4.92 kpsi	2.39 msec
A5 P(f)	196-210	20 k	(.210 v) 4.21 kpsi	2.18 msec
A6 SG1	346-360	100 k	(.212 v) 21.2 kμstrains	2.39 msec
A7 SG2	226-240	40 k	(.124 v) 4.96 kμstrains	2.37 msec
A8 SG3	241-255	100 k	(1.67 v) 167 kμstrains	2.41 msec
A9 SG4	256-270	100 k	(.167 v) 16.7 kμstrains	2.47 msec
A10 SG5	271-285	10 k	(.124 v) 1.24 kμstrains	2.42 msec

TABLE III (CONTINUED)

SENSOR	STORED	CONVERSION SCALE	PEAK VALUES	ARRIVAL TIME
A11 SG6	286-300	40 k	BAD READING	2.43 msec
A12 SG7	301-315	40 k	(1.17 v) 47 kμstrains	2.41 msec
B2 SG8	361-375	1.45 k	(.496 v) .72 kμstrains	2.45 msec
B3 SG9	376-390	2.87 k	(.499 v) 1.43 kμstrains	2.41 msec
B4 SG10	391-405	100 k	(.285 v) 28 kμstrains	2.40 msec
B5 SG11	NO DATA COLLECTED			
B6 SG12	406-420	10 k	(.037 v) .37 kμstrains	2.39 msec
B7 SG13	436-450	10 k	(.045 v) .45 kμstrains	2.34 msec

Notes: X" = Accelerometer, P(t) = Total Pressure Gage on Plate's Surface

P(f) = Free Field Pressure Gage

SG# = Strain Gage Number, (A/B)# = Honeywell Recorder A or B

v = volt

STORED = data storage locations on HP5451C disk

equating to 0.16 pounds of TNT at a real time of 2.05 msec. This value was compared to that of the plate's surface total pressure gage of 585 psi at time 2.13 msec. It is difficult to say why the peak surface pressure is less than the peak incident pressure but perhaps the time difference of 0.079 msec accounts for this degree of decay. This statement is predicated on the assumption that both pressure transducers were the same distance away from the charge. Selecting the value of 0.16 pounds of TNT, another EPSA computer run was made to determine the impact of this weight. Examining the EPSA output indicates the possibility that some permanent plate deflections may have resulted from the first shot. Maximum center plate deflection was calculated to be 0.0147 inches. Using the aluminum plate thickness of 0.25 inches, a ratio of deflection to plate thickness of 4% is attained. This is considered a small deflection and serves as a basis to ignore the impact of the first explosion. Another test performed to satisfy the hypothesis that the first shot did not have an overpowering effect on the test plate was a comparison of peak strains to yield strain. The typical yield strain for 6061-T6 aluminum is 4000 microstrains. The EPSA strains produced from a 0.016 pound TNT load are all well below yield. This indicates that the plate did not enter its plastic region.

Peak strain comparisons are provided in Figure 5.4. The values within the parentheses are EPSA predicted and the

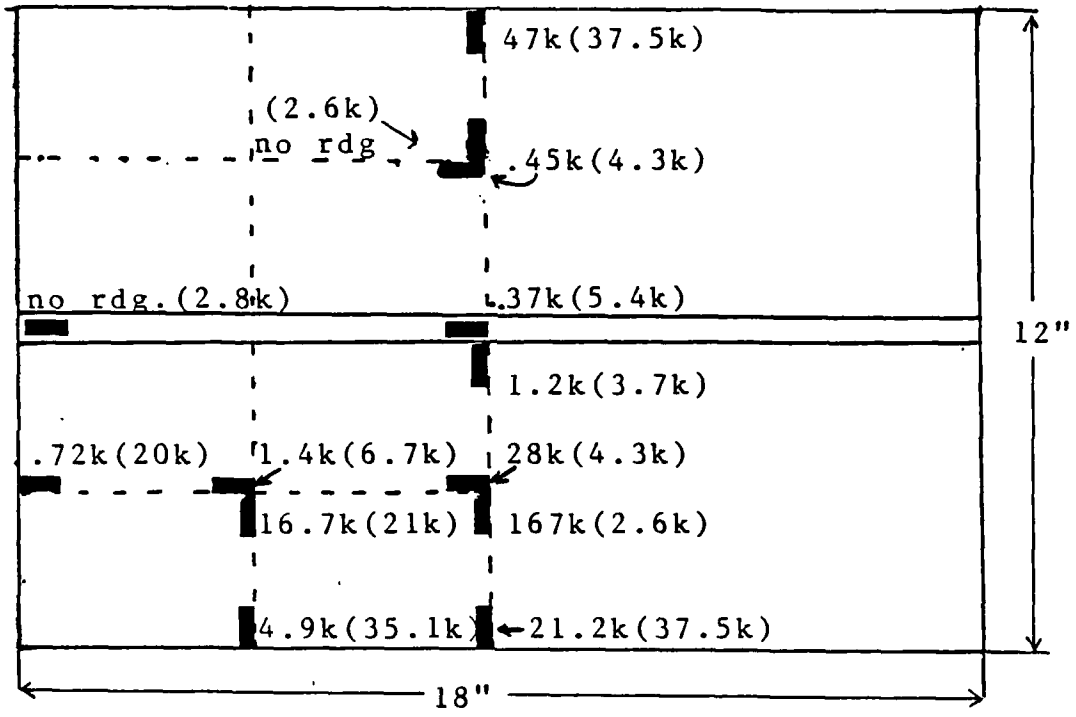

Note: Values have units of microstrains

Values in ( )'s are EPSA 8.0 lbs

Figure 5.4 Comparisons of Predicted to Actual Strains

ones outside represent experimental. It was disappointing to find such large discrepancies between gages. The measured peak values are haphazard, without any regard for consistency in reading higher or lower than expected. Two of the strain gages gave no output due to severed lead wires, and one indicated a reading beyond gage limits. Accelerometer magnitudes were equally useless. Both transducers registered values exceeding their maximum range. Sensor symmetry responses were investigated by comparing the outputs from three sets of strain gages and both accelerometers. Table IV gives the highlights of these comparisons. As alluded to earlier, the peak strain values are inconsistent but loading times are very close. Poor peak value comparisons add a great deal of uncertainty about the validity of the strain gage measurements.

TABLE IV

Symmetry Sensor Comparison

SENSOR	SHOT #1	SHOT #2
SG1&7	No comparisons due to bad SG1 values	Arrival Times within 0.7% Peaks off by factor of 2.2
SG3&6	Arrival times within 1.0% Peaks off by factor 2.1	Arrival times within 0.7% no comparison, bad SG6 value
SG10&13	not recorded	Arrival times within 2.4% Peaks off by factor of 62
X"	Arrival times within 0.3% Peaks off by factor 1.16	Arrival times within 2.7% Peaks off by factor 1.4

Notes: Peaks represent strains for the strain gages and G's for the Accelerometers (X")

The data pressure histories from shot two, enclosed in Appendix A, seem to be the most useful data obtained from this experiment. The peak surface total pressure sensor value of 4.922 kpsi is larger than the free field peak of 4.217 kpsi. Theoretically, plate total pressure should be twice as large as free field; but this is assuming an ideal rigid body response. An aluminum plate does not reflect perfectly, so any magnification between one and two is practical.

There does exist a time difference between pressure transducers. Prior to the structure's water entry, there was exactly a nine foot charge to transducer separation distance. A time comparison attempt was made to check whether these distances remained the same once submerged. The results of this comparison are shown in Table V. Theoretically, the

TABLE V

Pressure Sensor Time Comparisons

	SHOT #1		SHOT #2	
SENSOR	ARRIVAL	PEAK	ARRIVAL	PEAK
P(t)	2.116 msec	2.132 msec	2.390 msec	2.403 msec
P(f)	1.950 msec	2.024 msec	2.185 msec	2.213 msec
Time change	0.166 msec	0.109 msec	0.203 msec	0.190 msec
Distance	0.83 ft	0.54 ft	1.02 ft	0.95 ft

Note: Distance is computed assuming the speed of sound, 5 ft/msec

shock wave should have reached the plate at 1.8 msec, as computed from equation 2.2. The free field pressure

transducer, although identical to the other, does consistently give earlier signal readings. Table V indicates that a stand-off distance of exactly nine feet may not have been maintained between the charge and pressure transducers.

C. POST-SHOT EPSA TESTING

Initial comparison of EPSA predictions and experimental results indicated that the EPSA model was inaccurate or had some major prediction weaknesses. However, there are too many variables present in this UNDEX experiment to use such a gross generalization. The mechanics incorporated in EPSA are sound and based upon singularly proven theories. During an experiment, although ideal conditions are sought, they are seldom totally attained. Adopting a more realistic approach, further tests were conducted using EPSA. The main goal of the post-EPSA tests were to try to achieve the measured deflections using the code. Computer printouts of data results and PATRAN-G color slides were taken of the various EPSA runs, but they are too lengthy to include in this report. Appendix B provides sample EPSA input decks used for the different runs, should there exist an interest in recreating the data.

The following describes a list of post-EPSA tests that were conducted to try to imitate test results. First a 9.64 pound TNT run was made but the deflections were not significantly different from that of an eight pounder. Accounting for the fact that plate tears did occur, fundamental fracture

mechanics were attempted to be incorporated into EPSA. A change to the subroutine SM STIF allowed for modelling the plate with the stiffener ends cut. This provided a less rigid test panel but deflections remained symmetric. The stiffener ends were reattached and boundary conditions were written into the EPSA input deck to simulate actual plate tears along the top and side edges. The results from these cuts were quite interesting as this was the first time non-symmetric EPSA deflection patterns were produced. However, these cuts did not portray the time history or sequence whereby these tears developed. Finally, using data points from the second shot's classic free field pressure plot, actual pressure-time history information was inserted into a data deck. The pressure-time history run ignored charge weight and tearing conditions. The results were similar to a 9.84 pound charge. This was expected as it was from this graph that this weight was calculated. Using Table VI and Figure 5.5, a complete picture of EPSA deflection results are given. The term 'cut' in Table VI refers to the tear conditions observed from the second shot. None of the above steps reproduced the experimental results, but they did demonstrate some of EPSA's capabilities.

D. CONCLUSIONS AND RECOMMENDATIONS

After reviewing the results of this experiment and the others in this series, it is clear that stiffener tripping is not occurring. Stiffener tripping is not experienced due

TABLE VI

Comparison of Actual Deflection to EPSA Predictions

MARK	ACTUAL	8#	9.84#	0.16#	P-T	CUT 8#	CUT 9.84#	CUT P-T
1	.212	.061	.072	.004	.078	.143	.163	.700
2	.583	.328	.366	.031	.406	.618	.681	.679
3	1.195	.619	.676	.063	.688	.958	1.030	1.030
4	.757	.328	.366	.031	.406	-	-	-
5	.211	.061	.072	.004	.078	-	-	-
6	.448	.138	.156	.017	.115	.294	.328	.329
7	.939	.311	.341	.047	.317	.608	.661	.657
8	1.368	.353	.385	.050	.396	1.150	1.240	1.220
9	1.042	.311	.341	.047	.317	-	-	-
10	.524	.138	.156	.017	.115	-	-	-
11	.514	.072	.085	.005	.085	.480	.519	.505
12	1.008	.323	.361	.031	.395	.642	.707	.705
13	1.490	.601	.654	.063	.667	1.010	1.090	1.090
14	1.082	.323	.361	.031	.395	-	-	-
15	.514	.072	.085	.005	.085	-	-	-
16	.474	.061	.072	.004	.078	.438	.484	.473
17	.993	.328	.366	.031	.406	.618	.681	.679
18	1.424	.619	.676	.063	.688	.958	1.030	1.030
19	1.025	.328	.366	.031	.406	-	-	-
20	.590	.061	.072	.004	.078	-	-	-
21	.314	.138	.156	.017	.115	.133	.152	.159
22	.664	.311	.341	.047	.317	.360	.400	.408
23	.944	.353	.385	.050	.396	.515	.556	.551
24	.713	.311	.341	.047	.317	-	-	-
25	.383	.138	.156	.017	.115	-	-	-
26	.106	.099	.114	.011	.088	.097	.112	.122
27	.241	.174	.194	.024	.187	.172	.195	.206
28	.334	.172	.194	.024	.194	.236	.256	.258
29	.245	.174	.194	.024	.187	-	-	-
30	.129	.099	.114	.011	.088	-	-	-

NOTE: All deflections have units of inches
The mark number refers to the locations in Figure 5.5

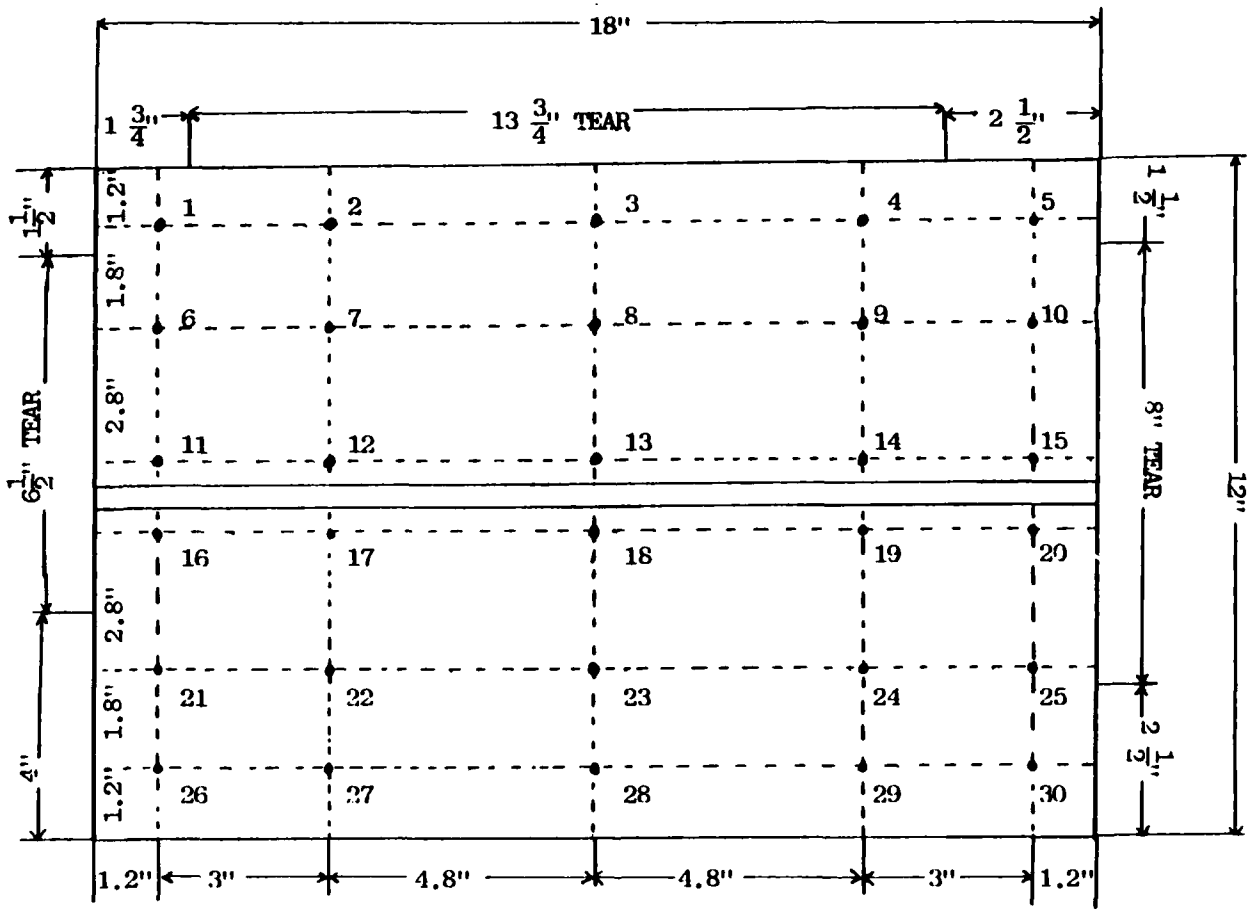

Figure 5.5 Deflection Locations

to the shearing of both ends of the stiffener. Numerical analysis does not predict the shearing or tearing along the sides. From the data, the sequence of fractures is not discernible. Knowing the order of fracture occurrence would give a better clue to plate responses. Additionally, EPSA predictions do not accurately forecast experimental results. In general the code predictions are lower than measured.

To observe stiffener tripping, the stiffener needs to have a compression mode throughout its entire length. Curvature must be introduced to the test panel. It is recommended for future studies to perform UNDEX testing using a stiffened shell model. This would provide all-around compression on the stiffener, promoting stiffener tripping instead of shearing. Also, it is necessary to incorporate tearing effects or fracture mechanics into the numerical analysis scheme. Symmetry loading conditions are not always observed from an UNDEX experiment and these need to be taken into account.

It is recommended that UNDEX testing be continued at NPS in order to improve experimental techniques and to acquire stiffener tripping data. Once tripping has been accomplished, then investigations can branch out to the gross shell responses of T and Z stiffeners. Improved stiffener technology would lead to a significant advancement in ship design.

APPENDIX A

HP-5451C FOURIER ANALYZER DATA HISTORIES

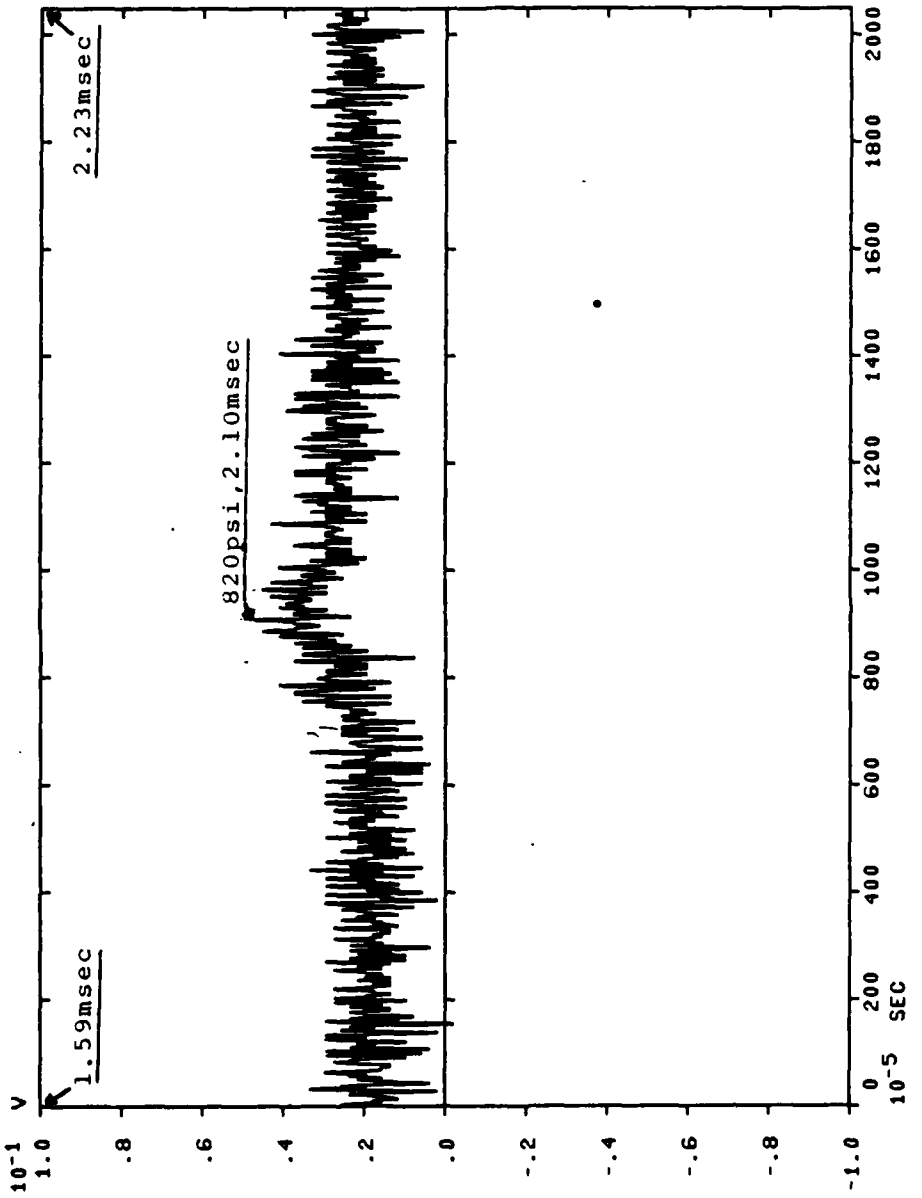

Figure A.1 Free Field Pressure Gage--Shot #1

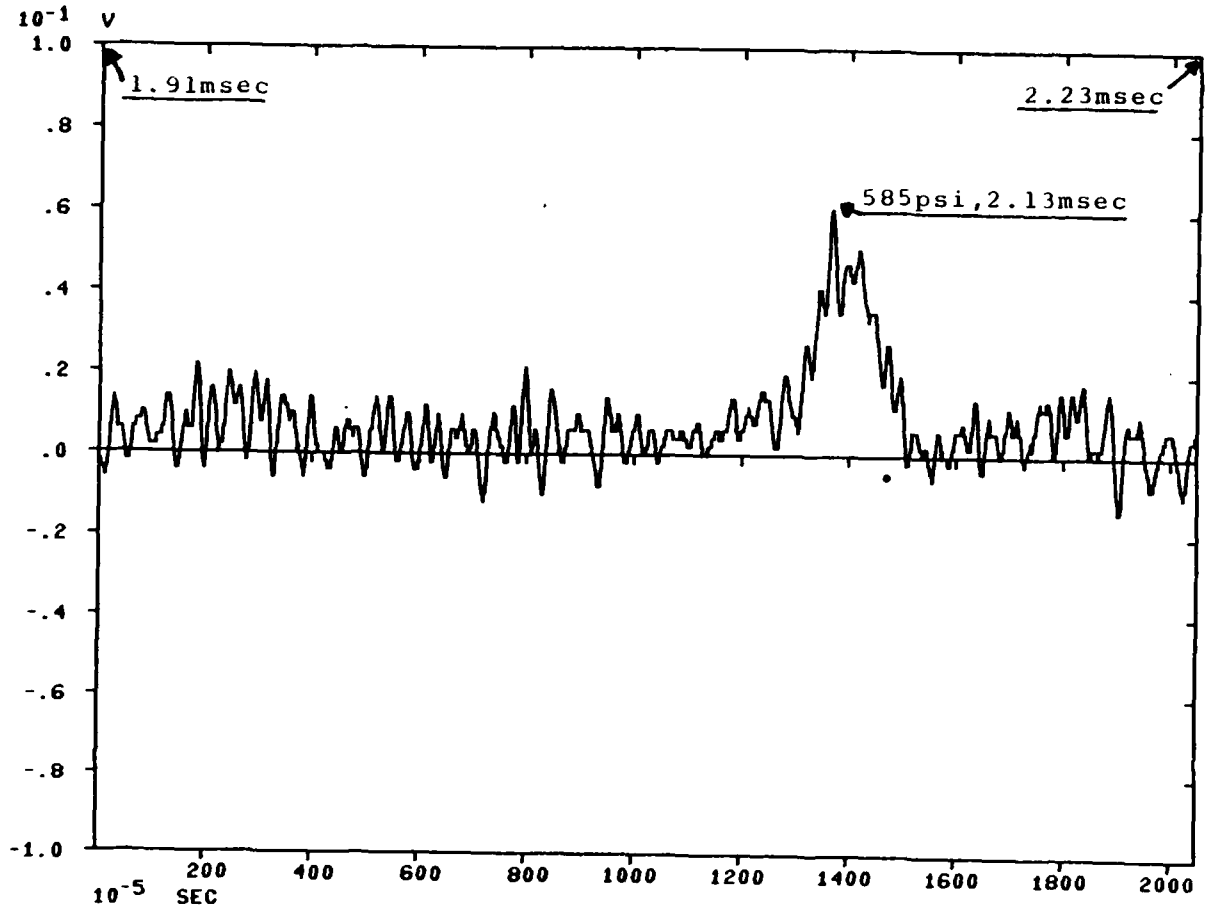

Figure A.2 Surface Total Pressure Gage--Shot #1

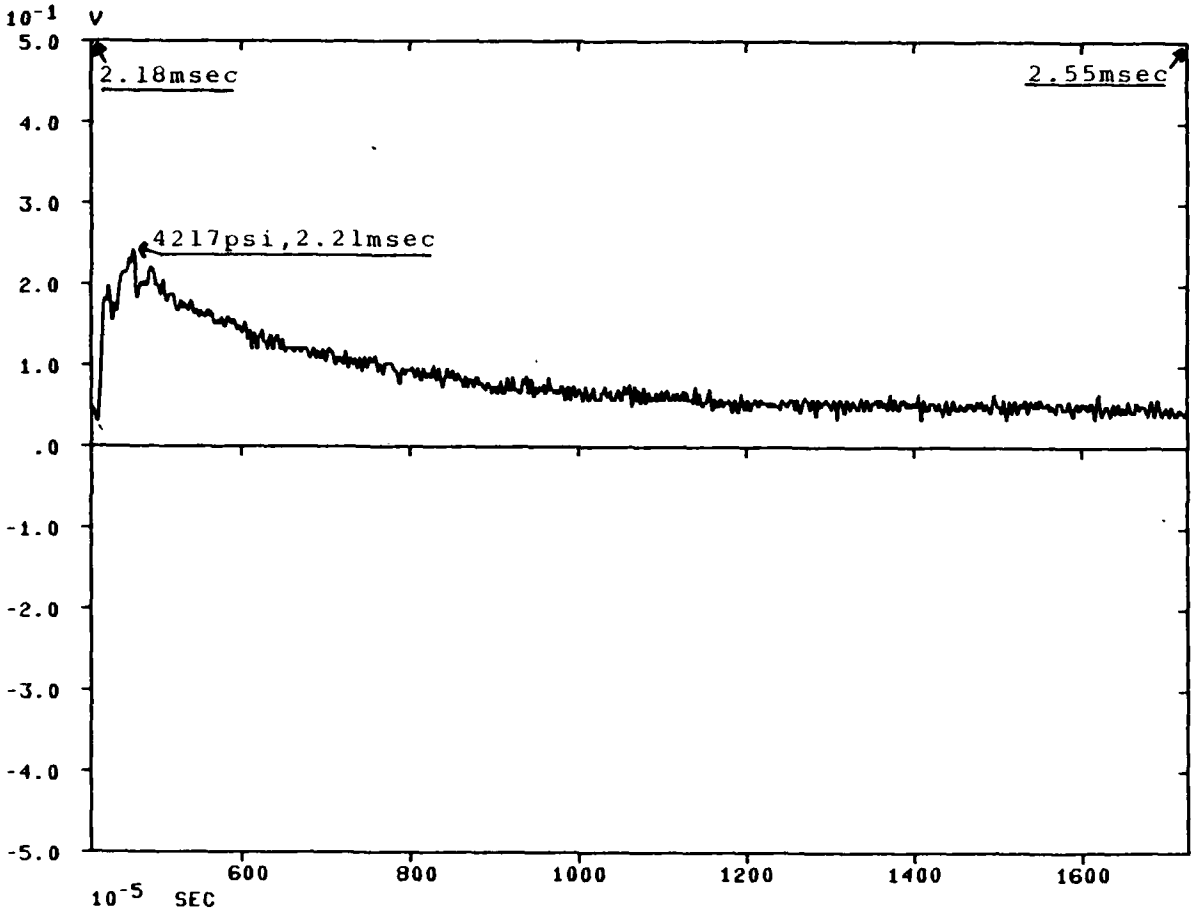

Figure A.3 Free Field Pressure Gage--Shot #2

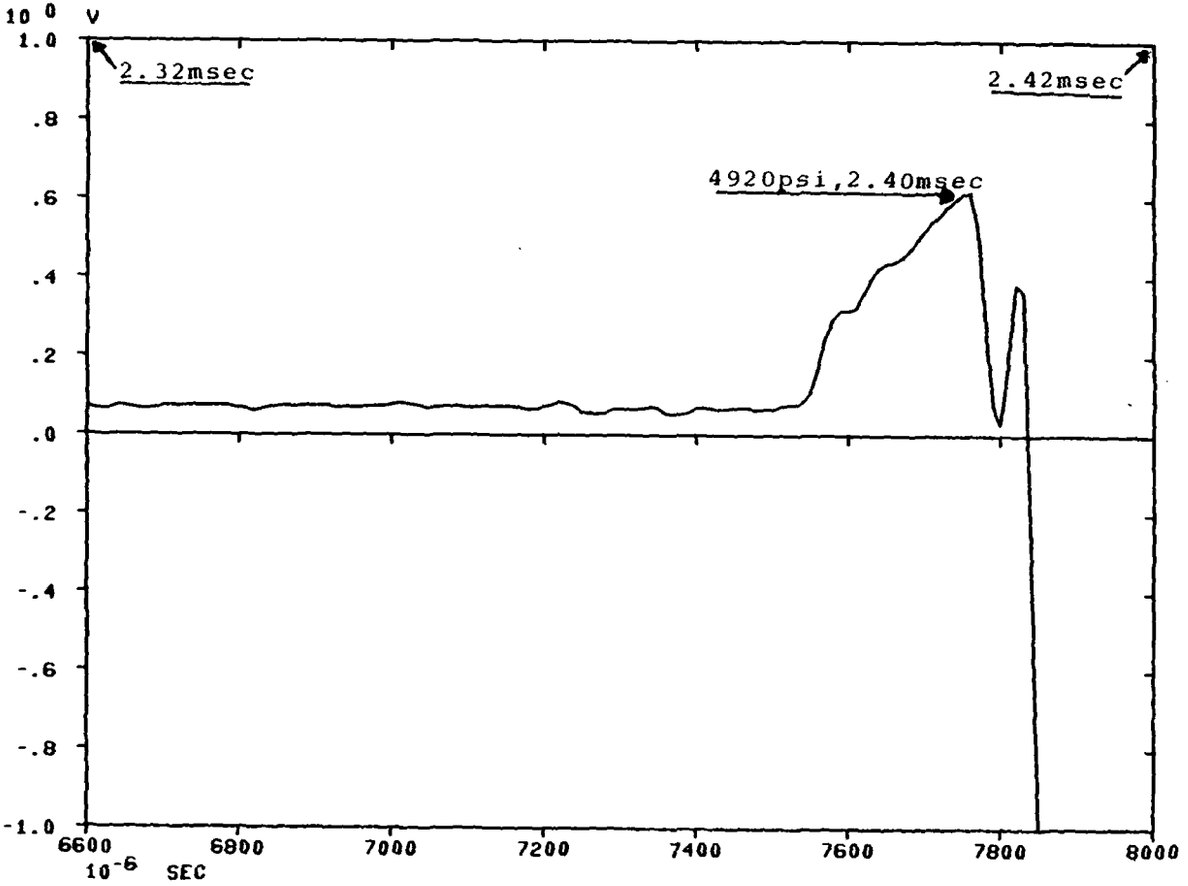

Figure A.4 Surface Total Pressure Gage--Shot #2

APPENDIX B

EPSA SAMPLE DATA DECKS

```
JL PLATE
2500 1 0 0 0 25 0 0 10 10
.000001 1 2500 25
1 1 14 15 13
15 25 4 1 1 0 4 24 40 30 1 1 0
0 0
10000000. .3 .000255 40000. .250 0. .00001
'STIF' 1 1 0
-1 1 2
416 0
1 0 0 0. 0.
16 1 0 9. 0.
-16 16 25 0 .48
0/
375 1 1 15 25
1 1 16 1 1 1 1 0
2 1 26 1 0 0 1 0
3 1 16 1 1 1 1 0
4 1 26 1 1 1 1 0
1 1 1 1 0. 0. 0.
0./
16 1 3 16 25 3 16 13 2 16 13 3/
1 1 1 1 1 2 1 1 4 1 1 5 15 1 1
15 1 2 15 1 4 15 1 5 3 13 1 3 13 2
3 13 4 3 13 5 8 1 1 8 1 2 8 1 4
8 1 5 1 7 1 1 7 2 1 7 4 1 7 5
3 3 1 3 3 2 3 3 4 3 3 5/
15 1 10 8 1 10 15 7 10 8 7 10 15 12 10
15 19 10 15 25 10 1 7 9 8 7 9 15 7 9
1 13 11 15 13 11 15 19 9 15 1 8 15 1 9
8 1 8 8 1 9 15 7 8 15 7 9 8 7 8
8 7 9 15 12 8 15 12 9 15 19 8 15 19 9
15 25 8 15 25 9 1 7 7 1 7 10 8 7 7
8 7 10 15 7 7 15 7 10 9 1 10 7 1 10
1 8 9 8 8 9 15 8 9 15 20 9 14 25 10/
16 23 3 8 23 3 3 23 3 16 20 3 8 20 3
3 20 3 16 17 3 8 17 3 3 17 3 16 10 3
8 10 3 3 10 3 16 7 3 8 7 3 3 7 3
16 4 3 9 4 3 3 4 3 16 13 3 1 13 3
9 2 3 14 12 3 14 13 3 14 14 3 15 12 3
15 13 3 15 14 3 16 12 3 16 14 3 7 13 3/
.48 .250 1.250
13 1/
0/
9.0     0.0000945    60000.0
1    108.166540    0.0554995     9.0
8.0    22505.0    1.13    0.058   -0.185 0.0012/
0/
```

Figure B.1 8 Pound EPSA Deck

```
JL PLATE
2500 1 0 0 0 10 0 0 1 1
.000001/
15 25 4 1 1 0 5 2 3 15 1 1 0
0 0
10000000. .3 .000255 40000. .250 0. .00001
'STIF' 1 1 0
-1 1 2
416 0
1 0 0 0. 0.
15 1 0 3. 0.
-16 16 25 0 .48
0/
375 1 1 15 25
1 1 16 1 1 1 1 0
2 1 25 1 0 0 1 0
3 1 15 1 1 1 1 0
4 1 25 1 1 1 1 0
1 1 1 1 0. 0. 0.
0./
16 1 3 16 1 2  16 13 2 16 13 3 1 1 2/
1 1 1 1 1 2/
15 1 10 8 1 10 15 7 10/
3 4 3 8 4 3 15 4 3 3 7 3 8 7 3
15 7 3 3 13 3 8 13 3 16 13 3 3 12 3
8 12 3 15 12 3 3 20 3 8 20 3 16 20 3/
.48 .250 1.250
13 1/
0/
9.0      1.0000345    50000.0
2    108.166547    0.9554935     9.0
7
0.0 3046.8 1.00079 2888.8 0.013125 3240.88 0.105625 2342.8
0.02125 4215.88 0.02153 2965.8 1.03422 3748.8
0.17598 250.0
)/
```

Figure B.2 Experimental Pressure--Time History Information

```
JL PLATE
2500 1 0 0 0 10 0 0 1 1
.000001/
15 25 7 1 1 0 3 1 1 15 1 1 0
0 0
10000000. .3 .000255 90000. .1875 0. .00001
'STIF' 1 1 0
-1 1 2
416 0
1 0 0 0. 0.
16 1 0 9. 0.
-16 16 25 0 .48
0/
575 1 1 15 25
1 1 16 1 1 1 1 0
2 1 26 1 0 0 0 1
3 1 4 1 1 1 1 0
3 5 16 0 0 0 0 1
4 1 9 1 1 1 1 0
4 10 23 0 0 0 0 1
4 24 26 1 1 1 1 0
1 1 1 1 0. 0. 0.
0./
16 1 1 16 1 2 16 1 3/
15 1 1/
15 1 7/
3 4 3 8 4 3 15 4 3 3 7 3 4 7 3
16 7 3 3 13 3 8 13 3 16 13 3 3 12 3
8 12 3 16 12 3 3 20 3 8 20 3 16 20 3/
.48 .250 1.25
13 1/
0/
9.0      0.0000945    60000.0
1    108.156540    0.0554985    9.0
9.84    22511.0    1.14    0.058    -0.145 0.00127
0/
```

Figure B.3 9.84 Pounds, Cut--Top and Sides

LIST OF REFERENCES

1. Butt, Lowell T., Naval Ship Shock Design Analysis, lecture notes for NPS Course ME4525, January 1984.

2. David, W. Taylor Naval Ship Research Center Report 79/064, Design Equations for Tripping of Stiffeners Under Inplane and Lateral Loads, by John C. Adamchak, October 1979.

3. Rentz, T.R. An Experimental Investigation into the Dynamic Response of a Stiffened Flat Plate Loaded Impulsively by an Underwater Shockwave, Master's Thesis, Naval Postgraduate School, Monterey, Ca., June 1984.

4. King, N.R. Underwater Shock-Induced Responses of Stiffened Flat Plates: An Investigation into the Predictive Capabilities of the USA-STAGS Code, Master's Thesis, Naval Postgraduate School, Monterey, Ca., December 1984.

5. David W. Taylor Naval Ship Research Tech Report 177-150C, Explosion Phenomena, by A.P. Misovec, June 1976.

6. Cole, Robert H., Underwater Explosions, Princeton University Press, 1948.

7. David W. Taylor Model Basin Report 1576, The Response of Ships to Underwater Explosions, by A.H. Keil, November 1961.

8. Atkatsh, R. and Daddazio, R., Supplement to the EPSA User's Manual, Weidlinger Associates, New York, NY, October 1982.

9. Lockheed Palo Alto Research Lab Notes, Underwater Shock Analysis (USA) Code, by Dr. John A. DeRuntz, Jr., February 1984.

10. Daube, R., Underwater Shock Response of Submerged Cylindrical Structures, Master's Thesis, Naval Postgraduate School, Monterey, Ca., December 1983.

INITIAL DISTRIBUTION LIST

		No. Copies
1.	Defense Technical Information Center Cameron Station Alexandria, VA 22314	2
2.	Library Code 0142 Naval Postgraduate School Monterey, CA 93943	2
3.	Chairman, Code 69 Department of Mechanical Engineering Naval Postgraduate School Monterey, CA 93943	1
4.	Professor Y.S. Shin, Code 69Sg Department of Mechanical Engineering Naval Postgraduate School Monterey, CA 93943	3
5.	Dr. R. Daddazio Weidlinger Associates 333 Seventh Avenue New York, New York 10001	1
6.	T.L. Geers Lockheed Missile and Space Company 3251 Hanover Street Palo Alto, CA 94304	1
7.	Cdr V. Campbell, USN Defense Nuclear Agency (SSPS) Washington, DC 20305	1
8.	Dr. G. Sevin Defense Nuclear Agency (SSPS) Washington, DC 20305	1
9.	S. Van Denk, Code U32 Department of the Navy Naval Surface Weapons Center, White Oaks Silver Springs, MD 20910	1
10.	Lcdr John R. Langan, USN 8833 Forestheights Dr. St. Louis, MO 63123	2

11. Mr. Vincent Langan 1
8833 Forestheights Dr.
St. Louis, M) 63123

12. Dr. James G. Langan, MD 1
2339 Chandabrook Dr.
Pelham, Al 35124

13. Mr. Louis Chaperlo 1
10592 Roxanna Dr.
St. Louis, MO 63128

14. Mr. Tom Christian, Code 69Rd 1
Department of Mechanical Engineering
Naval Postgraduate School
Monterey, CA 93943

15. Mr. R.B. Tussing, Code R15 1
Naval Surface Weapons Center
White Oak
Silver Springss, MD 20910

END

FILMED

7-85

DTIC